Nuclear translocation of LINE-1 encoded ORF1p alters nuclear envelope integrity and disrupts nucleocytoplasmic transport in neurons

Rania Znaidi, Olivia Massiani-Beaudoin, Philippe Mailly, Héloïse Monnet, Rajiv L Joshi, Julia Fuchs

Title:

Nuclear translocation of LINE-1 encoded ORF1p alters nuclear envelope integrity and disrupts nucleocytoplasmic transport in neurons

Authors:

Rania Znaidi[1], Olivia Massiani-Beaudoin[1], Philippe Mailly[2], Héloïse Monnet[2], Rajiv L. Joshi[1]* and Julia Fuchs[1]*

Affiliations:

[1]Interdisciplinary Research in Biology (CIRB), Collège de France, INSERM U1050/ CNRS UMR 7241, PSL Research University, 11 place Marcelin Berthelot, 75231 Paris Cedex 05, France.

[2]Orion Imaging Facility, Center for Interdisciplinary Research in Biology (CIRB), College de France, CNRS Unité Mixte de Recherche 724, INSERM Unité 1050, Labex Memolife, PSL Research University, Paris, France

***For correspondence:**

J.F. (Julia.fuchs@college-de-france.fr); R.L.J. (rajiv.joshi@college-de-france.fr)

Key words: Retrotransposons ; LINE-1 ; ORF1p ; nuclear envelope ; nuclear pore complex ; nucleo-cytoplasmic transport ; neurodegeneration.

Abstract

LINE-1 retrotransposons are emerging as possible culprits in neurodegenerative diseases. However, the molecular mechanisms underlying the pathogenic role of LINE-1 and their encoded proteins ORF1p and ORF2p are still not completely understood. While the endonuclease and reverse transcriptase activity of ORF2p has been associated with DNA damage and inflammation, no pathogenic role has yet been assigned to ORF1p. Using a neuronal model of oxidative stress displaying increased LINE-1 expression, we report here that ORF1p stress-dependently translocates into the nucleus, localizes to the nuclear envelope and directly binds to nuclear lamina (Lamin B1), nuclear pore complex (NUP153) components and nuclear import (KPNB1) proteins. Stress-dependent targeting of nuclear envelope components by ORF1p alters nuclear envelope integrity, disrupts nucleo-cytoplasmic transport and induces heterochromatin destructuration, which are key features associated with neurodegenerative diseases and aging. Interestingly, nuclear deformations and heterochromatin destructuration were restored by the small molecule Remodelin which also normalized nuclear ORF1p levels. This study thus reveals a retrotransposition-independent pathogenic action of ORF1p perturbing nuclear envelope barrier function.

Introduction

Repetitive sequences derived from transposable elements (TEs) represent 45% of the human genome, including non-LTR and LTR retroelements. Non-LTR retrotransposons of the Long Interspersed Element-1 (LINE-1) family have been the most active TEs in mammalian genomes and LINE-1-derived sequences represent almost 21% of the human genome which carries nearly 500000 LINE-1 copies [1]. Although most of these LINE-1 copies are remnants of past retrotransposition events and are truncated or mutated, the reference human genome still carries 146 full-length LINE-1 copies which can be autonomously active and competent for retrotransposition [2]. Full-length LINE-1 sense strand codes for two proteins, namely ORF1p and ORF2p, which are required for retrotransposition. ORF1p is an RNA binding protein and ORF2p encompasses reverse transcriptase and endonuclease activities. Since LINE-1 activation can lead to deleterious consequences such as DNA damage and genomic instability [3–6], senescence and inflammation [7,8], these TEs are repressed in most somatic cells at the transcriptional and post-transcriptional level. Failure of these repressive mechanisms can lead to the activation of LINE-1 and other TEs in the context of aging or human diseases like cancer.

Several recent studies have reported that TE activation might be linked to neurodegenerative diseases (NDs) such as Alzheimer's disease (AD), non-AD tauopathies, Parkinson disease (PD), Amyotrophic Lateral Sclerosis (ALS) and Huntington disease (HD) [5,9–14]. Although NDs present many common hallmarks such as pathological protein aggregation, synaptic and neuronal network dysfunction, aberrant proteostasis, cytoskeletal abnormalities, altered energy homeostasis, DNA and RNA defects, inflammation, oxidative stress and neuronal cell death [15,16], the genetic basis and the molecular and cellular mechanisms underlying neurodegeneration still remain elusive. In this regard, recent work from our group [5,17] and others [13,14,18] suggests that TE activation could directly contribute to neuronal

dysfunctions associated with NDs. Indeed, several pathogenic features of NDs might actually be linked to TE de-repression [19,20]. While the deleterious consequences attributed to the endonuclease and reverse transcriptase activities of LINE-1 ORF2p (i.e. DNA strand breaks, cytosolic single-stranded DNA inducing innate immune activation and inflammation) are beginning to be well documented, no particular pathogenic function has yet been assigned to ORF1p apart from its RNA chaperone property.

To directly address the consequences of endogenous full-length LINE-1 activation and increased LINE-1-encoded proteins in adult neurons, we used a neuronal model of acute oxidative stress displaying an increase in LINE-1 encoded ORF1p expression. Using this model, we uncovered a so far unrecognized pathogenic role of ORF1p in potentiating nuclear envelope (NE) barrier alterations induced by an acute oxidative stress. This suggests that stressed neurons are susceptible to ORF1p mediated NE perturbations leading to the amplification of NE dysfunctions which are novel emerging feature of many NDs.

Materiel and methods

Cell culture

The Lund Human Mesencephalic (LUHMES) cell line is a conditionally immortalized cell line. These cells are derived from the tetracycline-controlled, v-myc-overexpressing human mesencephalic cell line MESC2.10 [21,22]. The culturing and handling procedure of LUHMES cells were as described previously [21]. LUHMES cells can be differentiated into mature dopaminergic neurons. The differentiation was performed following the two-step protocol previously established [23]. Cell culture flasks, multi well plates and glass coverslips used for LUHMES culture were pre-coated by adding 50 µg/mL poly-L-ornithine (Sigma, P4957) diluted in 1X PBS (Phosphate buffered saline) for 1 h at 37°C, washed 3 times in 1X PBS, and

then incubated with 1 µg /mL fibronectin (Sigma, F0895) diluted in 1X PBS for 3 h minimum at 37°C to promote cell attachment. Uncapped flasks were air-dried before cell plating.

The base cell culture medium consisted of Advanced DMEM/F12 (Thermofisher 12634028), N2-Supplement (ThermoFisher Scientific, 17502048) and 2 mM GlutaMAX (ThermoFisher Scientific, 35050061) which was supplemented by 40 ng/ml recombinant human basic fibroblast growth factor FGF (Peprotech, 100-18B) during proliferation, at 37°C in 100% humidified air with 5% CO2 until 70%–80% of cellular confluence is reached.

The differentiation process was initiated by the shut-down of v-myc by adding 1 µg/ml doxycycline (Sigma, D9891) in the base medium supplemented with 2 ng/ml recombinant human glial-derived neurotrophic factor GDNF (Peprotech, 450-10) and 1 mM dibutyryl cyclic adenosine monophosphate sodium salt cAMP (Sigma, D0627). The pre-differentiated neurons were replated 48 h later at a defined density of 150 000 cells/well in 24-well plates or 10^6 cells/well in 6-well plates. To confirm successful generation of post-mitotic LUHMES, expression of neuronal and dopaminergic markers was assessed throughout the differentiation protocol, which lasts a total of 5 days (Fig. 1A; Suppl. Fig. 1A). All experiments were performed on day 5 of differentiation, at which point LUHMES cells were considered to be completely mature post-mitotic neurons.

Arsenite-induced oxidative stress

Stock of Sodium Arsenite solution ($NaAsO_2$) (Sigma-Aldrich, 1062771000, c= 0.05 mol/l) was stored at room temperature. Dilutions were carried out shortly before each experiment. Fully differentiated LUHMES cells (at day 5 of differentiation) were subjected to Arsenite during 1 h at 37°C at a concentration of 50 µM to induce oxidative stress.

Drug treatment

For LUHMES treatment with Remodelin drug (a gift from Dr. Raphaël Rodriguez), differentiated neurons at day 4 of differentiation, were incubated in fresh culture medium containing Remodelin (10 µM) or DMSO for 24 h and then subjected to oxidative stress using Arsenite (50 µM for 1 h at 37°C). For Stavudine treatment differentiated neurons (at day 4 of differentiation) were incubated in fresh culture medium containing Stavudine (10 µM) or NaCl for 24 h. The next day, cells were subjected to oxidative stress using Arsenite (50 µM for 1 h at 37°C).

Transfection methods

Adherent electroporation (Nucleofection): LUHMES cells were seeded at a density of 150 000 cells/well into 24-well plates already containing cover-slips pre-coated with poly-L-ornithine and fibronectine and were differentiated as described in Cell culture section. After 3 days of differentiation, cell culture medium was replaced by pre-warmed fresh medium and incubated for 1 h at 37°C prior to transfection. LUHMES cells were transfected by Nucleofection using the AMAXA 4D-Nucleofector® Y Unit (Lonza) which enables the direct Nucleofection (by electroporation) of cells in adherence in 24-well culture plates using the AD1 4D-Nucleofector™ Y Kit (Lonza, V4YP-1A24) for neuronal cells electroporation. The ER-100 program was the most appropriate to LUHMES cells in terms of transfection efficiency and viability and was used for all subsequent transfections. One Nucleofection sample contained 150 000 cells/well, 10 µg plasmid DNA (pcDNA3-ORF1-HA, a gift from Dr. John and Dr. Y. Ariumi) or 10 µg pmaxGFP vector and 350 µl AD1 4D-Nucleofector Y solution. The 24-well dipping electrode array (provided in the kit) was inserted into the plate and cells were transfected by using the ER-100 Nucleofector program. After nucleofection, AD1 solution was removed and the cells were immediately washed once with fresh medium and incubated in

humidified 37°C / 5% CO2 incubator. Media was not changed until analysis at day 5 of differentiation (48 h after transfection). Transfection efficiency (48 h after transfection) was monitored by fluorescence microscopy.

Protein extraction

After aspirating media, cells were washed one time with 1X PBS. 200 to 500 µl of 1X RIPA lysis buffer (50 mM Tris-HCL pH 8, 150 mM Nacl, 0,5% Sodium deoxycholate, 1% NP-40, 0,1% SDS) with 1X protease inhibitor (Sigma, 11836153001) was added to each well in the plate. Cells were scraped and lysates were transferred to a sterile microtube. The lysates were incubated on ice for 30 min and sonicated using the Bioruptor UCD-200 for 15 min (30s on/30s off) on ice at high power to shear contaminating DNA. After collecting the supernatant (avoiding the pellet) into new microtubes, protein concentration was determined using Pierce™ BCA Protein Assay Kit. Aliquot of lysates were stored at -20ºC avoiding multiple freeze/thaw cycles. Proteins were taken in 1X Laemmli buffer (250 mM Tris pH 6,8, 10% sodium dodecyl sulfate, 1,25% bromophenol blue, 5% β-mercaptoethanol, 50% glycerol) containing DTT, boiled 10 minutes at 95°C and stored at -20°C until analyzed.

Western blot analysis

A 1.5 mm NuPAGE 4-12% Bis-Tris-Gel (Invitrogen™M) polyacrylamide gel was used for Western blots. 10 ug of protein were loaded per well. Gel migrated in NuPAGE™ MES SDS Running Buffer (1X) (Invitrogen™M) for 55 minutes at 200 V. Gels were transferred into a methanol activated PVDF membrane (Immobilon) in a transfer buffer (Tris 25 mM, pH 8,3 and glycine 192 mM) during 1 h at 400 mA at 4°C. For blocking, 5% milk in TBST (0,2% Tween 20, 150 mM NaCI, 10 mM Tris pH:8) was used during 1 h at room temperature. The membranes were then incubated overnight with primary antibody anti-ORF1p 1:500 (Abcam, ab245249).

The membranes were incubated with anti-actin peroxidase antibody 1:20000 (Sigma, A3854) diluted in 5% milk in TBST, 1 h at room temperature on a shaker. The membranes were washed in TBST (1X) and incubated with secondary antibody including anti-rabbit HRP 1:2000 (Cell Signaling, 7074S) and anti-mouse HRP 1:2000 (Cell Signaling, 7076S) for 1 h at room temperature. After washing in TBST (1X), membranes were revealed using Clarity Western ECL Substrate (Bio Rad, #1705060) or Maxi Clarity Western ECL Substrate (BioRad, #1705062) in a LAS-4000 Fujifilm system.

Immunoprecipitation

For immunoprecipitation (IP) we used ORF1p (Millipore, MABC 1152) and IgG mouse (Thermofisher, #31903) antibodies. The antibodies were coupled to magnetic beads using the Dynabeads® Antibody Coupling Kit (Invitogen, 14311D) according to the manufacturer's recommendations. We used 8 µg of antibody for 1 mg of beads. The appropriate volume of buffer was added to the coupled beads to achieve a final concentration of 10 mg/ml.

LUHMES cells were plated at a density of $20x10^6$ cells in 2 T75 flasks and grown in differentiation medium for 5 days. One flask was treated with 50 µM Arsenite for 1 h. Control and treated cells were washed with 1X PBS and harvested using 1 ml of lysis buffer (10 mM Tris HCl pH 8, 150 mM NaCl, NP40 0.5% v/v, protease inhibitor 10 µl/ml) per T75 flask. Samples were sonicated for 15 min at 4°C, then centrifuged at 1200 rpm for 15 min at 4°C. The supernatants obtained were transferred to a new microcentrifuge tube and then separated into 3 tubes. One tube containing 50 µl of supernatant (1/10th of the test samples) was stored at 4°C until the samples were analyzed. The other two tubes containing 445 µl of the remaining supernatants were used for IP. Mouse IgG beads (75 µl) were added to one tube and ORF1p antibody beads (75 µl) to the other tube. Each of these two tubes was then diluted to 1.5 ml with buffer (10 mM Tris HCl pH8, 150 mM NaCl, 10 µl/ml protease inhibitor) to dilute the

NP40. The samples were then incubated overnight on a wheel at 4°C. Samples were then washed 3 times with 1 ml buffer (10 mM Tris HCl pH 8, 150 mM NaCl, 10 µl/ml protease inhibitor) using a magnet and then resuspended in 50 µl of the same buffer. The samples were boiled in Laemmli buffer (95°C, 10 min) and 20 µl of each sample were deposited on a 4-12% Nupage gel (Invitrogen, NP0336). Migration was carried out in MES SDS running buffer (Invitrogen, NP0002) for 45 min at 200 V. The gel was then transferred onto a PVDF membrane activated with methanol (Sigma, Immobilon-P 2659478) in glycine buffer (25 mM Tris, 200 mM glycine pH 8,3) for 1 h at 400 mA. The membranes were revealed using the primary antibodies anti-ORF1p rabbit 1:500 (Abcam, ab245249), anti-lamin B1 rabbit 1:1000 (Abcam, ab16048) or anti-KPNB1 rabbit 1:1000 (Cell Signaling, #51186), the secondary anti-rabbit HRP 1:2000 (Ozyme, 7074S) with the Maxi Clarity Western ECL Substrate kit (BioRad, #1705062). Analysis of immunoblotting images was performed manually using Fiji software.

RT-qPCR

Total RNA from $5x10^5$ lysed cells was extracted using RNeasy Plus Micro Kit (Qiagen, 74034) according to the manufacturer's instructions. The removal of contaminating genomic DNA (gDNA) was assessed by using the ezDNase kit (Invitrogen™, 11766051). After gDNA elimination, RNA (300 ng) was reverse transcribed using the All-In-One 5X RT MasterMix kit (Abcam, G592) for first-strand cDNA synthesis. The newly synthesized first-strand cDNA is ready for immediate real-time PCR analysis.

Quantitative PCR reactions were carried out in duplicates with SsoAdvanced Universal SYBR® Green Supermix (Biorad, 1725274) on a CFX Opus 384 (Bio-Rad, #12011452) with the following program: enzyme activation at 95°C 2 min, primer denaturation at 95°C, annealing at 57°C and primer extension at 72°C for 42 cycles. The following primers were used: HPRT (F: CAGCCCTGGCGTCGTGATTAGT; R: CCAGCAGGTCAGCAAAGA

AT); TBP (F: CAGCATCACTGTTTCTTGGCGT; R: AGATAGGGATTCCGGGAGTCAT) ; LINE-1 5'UTR (F: GTACCGGGTTCATCTCACTAGG R: TGTGGGATATAGTCTCGTG GTG), ORF1 (F: AGGAAATACAGAGAACGCCACAA) R: GCTGGATATGAAATTCTG GGTTGA), LINE-1 ORF2 (F: AAATGGTGCTGGGAAAACTG ; R: GCCATTGCTTTTGG TGTTTT), 3'UTR (F : GGGAATTGAACAATGAGATCAC; R: TATACATGTGCCATGC TGGTG).

Data were analyzed using the ddCt method and values normalized to hypoxanthine-guanine phosphoribosyl transferase (HPRT) or to glyceraldehyde-3-phosphate dehydrogenase (TBP) TATA-binding protein.

Proximity Ligation Assay (PLA)

The detection of the interactions between ORF1p and Lamin B1, NUP153 and KPNB1 were analyzed using proximity ligation Assay (PLA) method using Duolink® In Situ Red Starter Kit Mouse/Rabbit (Sigma, DUO92101). Cells were treated according to the manufacturer's instructions. After PLA, cells are mounted with a Fluoromount (Invitrogen™, 15586276). Fluorescence images were acquired using a Spinning Disk W1 Yokogawa imaging system.

Immunofluorescence

Immunostaining experiments were assessed at 1 h after Arsenite treatment. Stressed and control differentiated LUHMES cells cultured in 24-well plates (150 000 cells/well) were fixed with 4% paraformaldehyde (PFA) for 10 min. Immunofluorescence were performed overnight at 4°C after a 20 min permeabilization in 0,2% Triton X100 and incubation in blocking buffer (10 % bovine serum albumin BSA) for 1 h with the following antibodies: ORF1p 1:500 (Millipore, MABC1152 clone 4H1), TH 1:500 (Millipore, AB9702), Tuj1 1:1000 (Abcam, ab18207), Lamin B1 1:1000 (Abcam, ab16048), KPNB1 1:500 (GTX, 133733), NUP153 1:1000 (Novus

biological, NB100-93329), H4K20me3 1:1000 (Abcam, ab9053), HP1 1:1000 (Cell Signaling, #2623S), TDP-43 1:600 (Proteintech, 107-82-2AP), HA 1:1000 (Roche, 11867423001), RANGAP1 1:500 (Santa Cruz, sc-28322), ssDNA 1:500 (ENZO, (F7-26) ALX 804-192) diluted in the blocking buffer, overnight at 4°C. For ssDNA immunostaining, cells were fixed with PFA, followed by 24 h methanol incubation at -20°C, then incubated at 37°C for 4 h with RNaseA. Fluorescence secondary antibodies: Alexa Fluor 555, Alexa Fluor 488, Alexa Fluor 642, 1:2000 (ThermoFisher Scientific) were added for 1 h at room temperature. Nuclei were stained with Hoechst 1:2000 (Invitrogen, H3570). We used Fluoromount (Invitrogen™, 15586276). Cells were imaged by Spinning Disk W1 Yokogawa and STED Abberior Facility line imaging systems.

Quantification and image analysis

The quantification of ORF1p fluorescence was performed with a custom-written plugin (https://github.com/orion-cirb/Julia_Nucleus_Analysis) developed for the Fiji software [24], using Bio-Formats [25] and 3D Image Suite [26] libraries. Hoechst channel is downscaled by a factor 2, before detecting nuclei with the 2D-stitched version of Cellpose [27] (model = 'cyto2', diameter = 100, flow threshold = 0.4, cell probability threshold = 0.0, stitching threshold = 0.5). Segmented image is rescaled to original size and obtained 3D nuclei are filtered by volume to avoid false positive detections. Cells in ORF1p channel are detected in the same manner as nuclei. Then, each cell is associated with a nucleus having at least half of its volume in contact with it. Cells without any associated nucleus are filtered out. For each cell, ORF1p signal is analyzed in the following cellular compartments: cytoplasm, nucleus, outer and inner nuclear membranes and nucleoplasm (Fig. 2C, E). Compartmentalization is obtained using combinations of morphological operations (dilation, erosion and subtraction) of the cell and nucleus masks.

In each compartment, the integrated intensity of ORF1p is measured and normalized to ensure comparability across images. Normalization is done by subtracting the image background noise, estimated as the median intensity value of the minimum intensity Z-projection of the ORF1p channel. ORF1p foci are detected with Stardist 2D [28], applying a model trained on a dataset of 1950 images of foci. The following settings are used: percentile normalization = [0.2 - 99.8], probability threshold = 0.2, overlap threshold = 0.25. ORF1p foci are then labeled in 3D and filtered by volume. The number of foci, their volume and their normalized integrated intensity are computed in each cellular compartment. Results are provided as an Excel file.

To quantify nuclear deformation, another custom plugin (https://github.com/orion-cirb/HA_ORF1P_Prot/) was developed for the Fiji software, that uses the same libraries listed above, CLIJ [29] and Find Focused Slices (https://sites.google.com/site/qingzongtseng/find-focus?authuser=0). In brief, best focussed slice in the stack is selected. Nuclei are detected on this slice with Cellpose 2D (model = 'cyto2', diameter = 120, flow threshold = 0.4, cell probability threshold = 0.0), filtered by area and their circularity is computed. For each nucleus, ORF1p integrated intensity is analyzed in the following compartments: nucleus, outer and inner nuclear membranes and nucleoplasm. Compartments are obtained with the same combinations of morphological operations than previously described.

In case a HA-ORF1p channel is provided, cells are detected on the best focussed slice with Cellpose 2D (model = 'cyto2', diameter = 200, flow threshold = 0.4, cell probability threshold = 0.0) and filtered by area. Nuclei having at least one pixel in contact with a HA-ORF1p cell are considered as HA-ORF1p+, other nuclei as HA-ORF1p-. The intensity quantification of other markers than ORF1p was also performed with this plugin.

Statistical Analysis

Data were obtained from independent experiments. The number of cells analyzed in each experiment is described in corresponding figure legends. Data analysis was performed using GraphPad Prism 8. Shapiro Wilk normality tests were performed prior to the statistical test. Two-tailed Student's t-test or One-way ANOVA with Tukey's multiple comparisons test were used to determine statistical significance. Data are expressed as mean ± standard error of the mean (SEM). The significant threshold was defined as $p<0.5$ and depicted as follows on all graphs: *$p < 0.5$, **$p < 0.01$, ***$p < 0.001$, ****$p < 0.0001$.

Results

Stress-induced activation of LINE-1 in human post-mitotic dopaminergic neurons

LUHMES cells represent a robust model to investigate the molecular and cellular mechanisms leading to neurodegeneration [30–32]. LUHMES cells were differentiated into post-mitotic neurons according to the experimental paradigm [21–23] displayed in Fig. 1A and Suppl. Fig. 1A. These cells acquire a mature dopaminergic neuronal phenotype as revealed by immunostaining for the neuronal marker Tuj1 (β-III tubulin) and the dopaminergic marker TH (Tyrosine hydroxylase) at day 5 of differentiation as shown in Figure 1B and quantified in Supplementary Figure 1B. The dopaminergic phenotype of these cells was further confirmed by analyzing TH protein expression by Western blot at different days of differentiation (Suppl. Fig. 1C). Surprisingly, but as previously observed in mouse dopaminergic neurons [5], full-length LINE-1 elements are expressed at steady-state in human dopaminergic neurons as revealed by immunostaining for the LINE-1 ORF1p protein (Fig. 1B). Human ORF1p, as mouse ORF1p, shows a predominant cytoplasmic expression pattern. Oxidative stress is a common feature of aging [33–35], cancer [36] and NDs [37–40] and has been associated with LINE-1 activation [41–43]. To

generate a human neuronal model of endogenous LINE-1 activation, we induced oxidative stress in differentiated dopaminergic neurons with low-dose arsenite ($NaAsO_2$; 50 μM) for 1 hour at day 5 of differentiation as described in Figure 1A. This treatment did not affect the neuronal and dopaminergic phenotypes as shown by Tuj1 and TH immunofluorescence quantification (Suppl. Fig. 1D, E) and triggered no apparent cell death. Oxidative stress increased the expression of LINE-1 in human neurons as revealed by Western blot and immunofluorescence analysis of LINE-1 ORF1p protein (Fig. 1C, D). LINE-1 RNA quantification by RT-qPCR using several primers targeting different regions of the LINE-1 sequence also showed an up-regulation of LINE-1 transcripts (Suppl. Fig. 1F). In order to test LINE-1 encoded protein activity, we analyzed two known consequences of ORF2p activity (for which no effective antibodies are available). Increased LINE-1 ORF2p has been previously reported to induce DNA damage due to the endonuclease activity [3–5]. Upon oxidative stress, differentiated human dopaminergic neurons displayed increased DNA damage as quantified by an increase in γH2AX (Phosphorylated histone H2AX)-positive foci, which decreased in the presence of Stavudine, an inhibitor of the reverse transcriptase of LINE-1 ORF2p (Fig. 1E). The reverse transcriptase activity of LINE-1 ORF2p has also been reported to generate the accumulation of single-stranded DNA (ssDNA) in the cytosol leading to inflammation [6,44]. We also observed an increase of ssDNA foci volume and intensity in the cytosol of stressed neurons (Suppl. Fig. 2A). Full-length LINE-1 and its encoded proteins are thus expressed at steady-state in human dopaminergic neurons, are inducible by oxidative stress and functionally active. This *in vitro* model therefore represents a valuable tool to investigate cellular effects of LINE-1 activation mediated by the encoded proteins.

ORF1p localizes to the nuclear envelope and translocates into the nucleus upon oxidative stress

We next investigated the precise cellular localization and quantity of ORF1p upon stress using confocal imaging (Fig. 2A). ORF1p was predominantly cytoplasmic both in steady-state as well as in stress conditions and showed both, diffuse and dot-like patterns. Surprisingly and against the current assumptions [45], we observed the presence of ORF1p in the nuclear compartment and an accumulation of ORF1p at the nuclear periphery both at the outer and the inner NE as distinguishable by Hoechst DNA staining (Fig. 2A, B). We further quantified ORF1p intensities using an automated deep-learning based quantification script developed in-house as schematized (Fig. 2C). This script allows for the quantification of immunofluorescence intensities, dot numbers and volumes in pre-defined cellular compartments including the nucleus and the cytosol. The increase in staining intensities was accompanied by a rearrangement of staining patterns as revealed by an increase in ORF1p-positive dot numbers and volumes, both in the cytoplasm and the nucleus (Fig. 2D), indicating a possible condensation of LINE-1 ORF1p in stress conditions.

As ORF1p appeared to accumulate along the NE, the script was further applied to analyze ORF1p intensity in more detailed compartments including the outer NE, the inner NE and the nucleoplasm (not including the inner NE) (Fig. 2E). The quantification showed a significant increase of ORF1p in both the inner and outer NE and in the nucleoplasm (Fig. 2F).

In summary, ORF1p immunostainings using an unbiased image quantification method revealed increased LINE-1 ORF1p levels in the cytoplasm, in the nucleus, and in the inner and outer NE, indicating a general increase of ORF1p, the accumulation of ORF1p at the NE, a rearrangement of ORF1p in a dot-like manner particularly in the cytoplasm and a significant nuclear translocation upon stress.

ORF1p targets nuclear envelope components upon oxidative stress

To confirm ORF1p localization to the inner NE, we performed co-immunostainings for ORF1p and Lamin B1, a nuclear lamina protein which decorates the inner NE and plays a key role in the maintenance of nuclear architecture. These experiments revealed the colocalization of ORF1p and Lamin B1 at the inner NE which increased upon stress. This colocalization is particularly visible at the level of lamina invaginations (Fig. 3A). Co-immunoprecipitation experiments confirmed the interaction between ORF1p and Lamin B1 under stress conditions (Fig. 3B). Direct binding of ORF1p to Lamin B1 was further examined by proximity ligation assay (PLA). The results obtained indicate a direct interaction between ORF1p and Lamin B1 at the nuclear periphery upon stress (Fig. 3C) in line with the colocalization signals observed by co-immunostainings (Fig. 1A). However, direct interaction of ORF1p and Lamin B1 is also detected in the nucleoplasm of neurons and PLA signal quantification confirmed an increase of the number of dots (= direct interaction events) at the inner NE but also in the nucleoplasmic compartment (Fig. 3D). This suggests a possible scenario in which the stress-induced nuclear translocation of ORF1p and direct ORF1p binding to Lamin B1 induces Lamin B1 mislocalization from the inner NE to the nucleoplasm.

Previous studies have shown that ORF1p interacts with importin beta family members (*i.e*, KPNB1) [46], which could mediate its nuclear translocation using nuclear pore complexes (NPCs). To examine whether ORF1p nuclear translocation observed in human neurons upon oxidative stress (Fig. 2B) might depend on KPNB1 mediated import, we performed co-immunostaining of ORF1p with the importin KPNB1 or NUP153 (a nucleoporin of the nuclear basket), a core NPC protein shown to interact with KPNB1 [47]. The results shown in Figure 3E indicate the colocalization of ORF1p with KPNB1 and NUP153 at the NE suggesting that nuclear translocation of ORF1p in human neurons upon oxidative stress might indeed be mediated by these proteins. Our results are in line with previous reports describing that KPNB1

may be involved in active nuclear import of LINE-1 ORF1p [48]. In addition, several cytoplasmic ORF1p-positive foci colocalize with KPNB1 (Fig. 3E) suggesting possible sequestration of this importin with ORF1p. Direct interaction of ORF1p with KPNB1 and NUP153 was further confirmed by PLA (Fig. 3F). PLA signal of ORF1p and KPNB1 interaction is not affected by oxidative stress (Fig. 3G), whereas the direct interaction between ORF1p and NUP153 is clearly increased in stress condition (Fig. 3H). These results suggest that ORF1p directly interacts with components of the inner NE and the nucleo-cytoplasmic transport (NCT) machinery and might mislocalize these proteins interfering with their physiological functions in nuclear architecture and NCT function. This let us to investigate whether ORF1p localization to the NE and direct protein-protein interaction with Lamin B1, KPNB1 and NUP153 might affect NE morphology and/or NCT efficiency.

Nuclear ORF1p accumulation correlates with nuclear envelope alterations

Lamin B1-based staining of the inner nuclear lamina of human dopaminergic neurons revealed various NE dysmorphologies including nuclear invaginations and blebbing which appeared upon oxidative stress (exemplified in Fig. 4A). It is noteworthy that nearly 70% of stressed cells presented such deformations (Fig. 4B). Co-immunostaining for ORF1p and Lamin B1 revealed the accumulation of ORF1p at the level of NE invaginations and blubs, which is clearly observable in STED acquired 3D images and 3D reconstituted images (Fig. 4A). Nuclear dysmorphology was accompanied by increased Lamin B1 levels at the inner NE but even more so in the nucleoplasm of stressed cells (Fig. 4C), again suggesting a mislocalization or relocalization of Lamin B1 possibly as a result of direct protein interactions with ORF1p. The degree of NE distortion (expressed as a circularity index) was analyzed using an automated script (detailed in the Materiel and Methods section) which measures nuclear circularity using Lamin B1 staining as a mask. This analysis showed a significant decrease of nuclear circularity

in stressed cells (Fig. 4D). Importantly, the degree of nuclear distortion (the lower the index, the higher the distortion) was significantly correlated with the intensity of nuclear ORF1p staining (thus nuclear ORF1p quantity) both in the nucleoplasm and in the inner NE (Fig. 4E). This correlation strongly suggests that nuclear ORF1p translocation and accumulation in the nucleoplasm and at the inner NE, at least in part, is functionally involved in the occurrence of nuclear dysmorphologies observed in neurons upon oxidative stress. It is noteworthy that ORF2p activity inhibitor (Stavudine) which prevented ORF2p induced DNA strand breaks (Fig. 1E) did not have any effect on nuclear circularity, or Lamin B1 delocalization, nor on ORF1p nuclear and cytoplasmic levels (Suppl. Fig. 3A-C). This suggests that the effect observed is not due to ORF2p activity.

Since nuclear lamina plays an important role in anchoring heterochromatin at the inner NE (= nuclear lamina), we examined whether the observed alteration of the nuclear lamina is accompanied by heterochromatin disorganization by immunostaining for the heterochromatin markers HP1 (heterochromatin marker protein-1) and the repressive histone mark H4K20me3 (histone H4, trimethylated on lysine 20) in control and stressed cells. HP1 was significantly depleted from the inner NE (Fig. 4F) and H4K20me3 levels decreased in stress conditions (Fig. 4G) suggesting possible decondensation or detachment of heterochromatin from the inner NE.

Nuclear envelope targeting by ORF1p is accompanied by nucleo-cytoplasmic transport defects

In view of the interaction of ORF1p with KPNB1 and NUP153 reported above, we examined whether the accumulation of ORF1p at the NE could lead to NCT deficiencies. Immunostainings and subsequent quantification of intensity, distribution and localization of KPNB1 showed an accumulation of KPNB1 in the cytoplasm, as revealed by an increase in the intensity of KPNB1. We also observed a change in KPNB1 distribution, as revealed by an

increase in the number of counted dots and their volume in the cytoplasm (Fig. 5A) indicating a possible alteration of its function. To examine whether these changes in KPNB1 upon stress were associated with NCT defects, we first analyzed the localization of a major nucleo-cytoplasmic transport protein, RANgap1, by immunostaining. The GTPase activity of this protein is involved in maintaining the RAN gradient required for NCT and its delocalization is associated with NCT defects [49]. RANgap1 accumulated in the cytoplasm, shown by increased intensity, number and dot volume in the cytoplasm (Fig. 5B) which is indicative of an alteration of NCT. Disruption of NCT can lead to the abnormal localization of the RNA binding protein TDP-43, a predominantly nuclear protein. *TARDBP* mutations are causal in familial forms of FTD and ALS and a change from its predominantly nuclear to cytoplasmic localization has been observed in several NDs. Current consensus suggests that TDP-43 misdistribution leads to a pathological gain-of-function in the cytoplasm and loss-of-function in the nucleus [50,51] contributing to cellular dysregulation culminating in neurodegeneration. We therefore performed immunostainings for TDP-43 which revealed the presence of TDP-43-positive foci in the cytoplasm under stress conditions which were absent in non-stressed controls. Quantification showed that the intensity as well as the number and volume of TDP-43 positive dots were increased in the cytoplasm in stressed neurons (Fig. 5C). The quantification of the nucleoporin NUP153 showed an abnormal intranuclear and cytoplasmic accumulation of NUP153 in stress conditions (Fig. 5D).

Attempts to establish a causal link between the increase of LINE-1 ORF1p and NE alterations and NCT defects using siRNA were technically not successful. We therefore performed LINE-1 ORF1p gain of function experiments to examine whether increased ORF1p (and only ORF1p) could lead to the above-described effects in the absence of stress.

ORF1p overexpression leads to nuclear envelope dysmorphology and nucleo-cytoplasmic transport defects in the absence of oxidative stress

Dopaminergic neurons were nucleofected at day 3 of differentiation with a plasmid encoding either ORF1-HA or GFP control and analyzed 48 h later. Co-immunostainings for HA and Lamin B1 showed the presence of HA-ORF1 in the nucleus and at the inner NE, colocalizing with Lamin B1 (Fig. 6A). HA-ORF1 transfected cells displayed pronounced NE deformations as revealed by Lamin B1 staining (Fig. 6A), decreased circularity and increased nucleoplasmic Lamin B1 levels compared to GFP expressing cells (Fig. 6B). Interestingly, nuclear circularity was highly correlated with the nuclear intensity of HA-ORF1 in transfected cells (Fig. 6B), strongly suggesting a causal link between ORF1p nuclear localization and NE dysmorphology. Neurons transfected with HA-ORF1 also presented increased levels of RANgap1 in the cytoplasm and TDP-43 in both the cytoplasm and nucleus compared to GFP expressing cells (Fig. 6C-F). These results indicate that overexpression of ORF1p, in the absence of stress, is sufficient to induce NCT defects and NE dysmorphology in human dopaminergic neurons.

Rescue of nuclear envelope dysmorphology under stress conditions by Remodelin

NE morphology is disrupted during aging [52] and in premature aging syndromes caused by laminopathies [53,54] including progeria syndromes [55]. In Hutchinson-Gilford progeria syndrome (HGPS), nuclear integrity was shown to be restored by the small molecule “Remodelin”, an inhibitor of the acetylase-transferase protein NAT10 [56] but whether this molecule is efficient in restoring misshapen nuclear morphology in cell types other than fibroblasts or epithelial cells was not known. We therefore examined whether NE dysmorphology induced by ORF1p under oxidative stress in human neurons could be restored by Remodelin. NE deformations (i.e invaginations) were clearly restored in cells pre-treated with Remodelin for 24 h (Fig. 7A, B). Quantification showed that the decrease of nuclear circularity following arsenite treatment was

restored by Remodelin (Fig. 7B), which was paralleled by a reduction of nucleoplasmic Lamin B1 levels quantified in Figure 7B. In order to investigate whether Remodelin treatment had an influence on ORF1p levels, we performed ORF1p immunostainings on cells treated or not with Remodelin. Arsenite-induced nuclear ORF1p increase was completely normalized in the presence of Remodelin, both at the inner NE and in the nucleoplasm (Fig. 7C) Interestingly, in these conditions cytoplasmic ORF1p levels remained unchanged at an expected higher level than non-stressed controls. Since Remodelin has been reported to restore a "juvenile" chromatin state in Progeria models [56,57], we examined H4K20me3, known to repress LINE-1 elements [58,59]. As shown in Figure 7A, H4K20me3 immunostaining was significantly decreased following stress and restored with Remodelin treatment as confirmed by quantification of H4K20me3 intensity in the nucleus (Fig. 7D). This suggests that the decrease of nuclear ORF1p upon Remodelin treatment in stressed cells might induce indirect blockage of nuclear ORF1p translocation. Alternatively, this decrease could also be due to a transcriptional inhibition of LINE-1 or a consequence of deposition of H4K20me3 at LINE-1 loci.

Discussion

In recent years, TEs have emerged as possible new pathogenic players in NDs [5,10,13,19,20,60–62]. However, the mechanisms through which LINE-1 might contribute to the pathogenesis of NDs still remain poorly understood potentially implicating cis-genetic or epigenetic, LINE-1 RNA or LINE-1 protein-mediated effects. Concerning the latter, the study of potential pathogenic effects of LINE-1 ORF2p has received most attention due to its enzymatic activities as an endonuclease and reverse transcriptase while ORF1p has widely been reduced to an RNA chaperone with cis-preference for its own RNA and a necessary component of the LINE-1 ribonucleoprotein particle (RNP) for retrotransposition. Previous work suggests that ORF2p is

not only a source of genomic instability [3–6,20], but can also trigger the innate immune response through reverse transcription of RNA generating cytoplasmic ssDNA [6,8,44]. While ORF2p reverse transcriptase activity can be targeted by inhibitors (nucleoside reverse transcriptase inhibitors, NRTIs, i.e. Stavudine), the analysis of ORF2p protein expression and localization remains challenging due to a lack of efficient antibodies and/or its lesser abundance compared to ORF1p (1 ORF2p for 240 ORF1p molecules per LINE-1 RNP [63]. In contrast, no inhibitor has been identified to target ORF1p activity, but effective antibodies are available to explore its expression and subcellular localization in pathological situations. However, a better understanding of the implication of ORF1p in the LINE-1 life cycle and beyond is interesting as accumulating data suggests that full-length LINE-1 are expressed, predominantly in epithelial cancers [64] but also at steady-state in mouse neurons [5], human neurons [65] and post-mortem brain tissues [66].

Using a human neuronal model of oxidative stress which displays increased LINE-1 activity as monitored by an increase in ORF1p expression and ORF2p-dependent genomic instability, we observed not only an increase of ORF1p in the cytoplasm, but also a striking translocation of ORF1p to the nucleus. Current consensus postulates that LINE-1 encoded proteins enter the nucleus only during cell cycle [45] which thus would exclude the presence of LINE-1 proteins in the nucleus of non-dividing cells including post-mitotic neurons. However, others have reported the presence of ORF1p in the nucleus in human cells in neurodegenerative context [67]. We also observed ORF1p staining in the nucleus of human dopaminergic neurons *in vitro* and in mouse dopaminergic neurons *in vivo* even at steady-state [5], and oxidative stress dramatically increases the nuclear translocation of ORF1p. The most probable mode of import for ORF1p is the importin-beta pathway. Indeed, ORF1p, as we show here in neurons and others have shown in HeLa cells [46] binds directly to the importin beta family member KPNB1, which is a transport mediator carrying cargo proteins through the NPC. This importin-assisted mode

of nuclear entry is widely used by several viral proteins [68,69], certain retrotransposons (i.e Ty1 [70], LINE-1 ORF1p itself [48]) but also a pathological form of Tau which aggregates in neurodegeneration [71]. The binding of ORF1p to KPNB1 does not increase under stress condition indicating that the stress-induced increase of ORF1p nuclear translocation probably requires other protein partners. It is noteworthy that ORF1p, in a stress-dependent manner, accumulates both at the outer NE and the inner NE which corresponds to the nuclear lamina and co-localizes with and binds directly to the NPC protein NUP153. This suggests a NUP153-dependent nuclear import of ORF1p under stress. Indeed, NUP153 binding of cytoplasmic proteins can mediate nuclear import of proteins [72]. ORF1p and NUP153 interaction might be favored by KPNB1, which also binds NUP153 [72]. However, both pathways also interact [73] making it difficult to dissect the precise mechanisms.

The small transcriptional increase in LINE-1 RNA following arsenite treatment suggests that the overall increase in ORF1p could be partially transcriptional and partially post-transcriptional, possibly by releasing LINE- 1 RNA stored in P-bodies for translation [74,75]. Once ORF1p translocates to the nucleus, it accumulates at the inner NE by directly binding to Lamin B1 in a stress-specific manner. This targeting of the inner NE by ORF1p is paralleled by NE dysmorphology including invaginations and blebs which significantly correlated with ORF1p intensity, both in the nucleus and the inner NE, suggesting that it is the stress-dependent nuclear translocation of ORF1p and the direct binding to Lamin B1 that participate in NE dysmorphology. A direct functional role of ORF1p in NE dysmorphology independent of oxidative stress is further supported by direct ORF1p gain of function experiments showing that neurons over-expressing ORF1p (and not ORF2p) display a significant decrease of nuclear circularity. These experiments also suggest that NE dysmorphology is mediated by the nuclear presence of ORF1p alone and does not rely on the presence of the entire RNP or ORF2p. NE dysmorphology is associated with NCT deficiencies [76] and both have been described to be

disturbed in the context of NDs [51,77–83]. Indeed, targeting of the NE by ORF1p in neurons was accompanied by NCT deficiencies as revealed by the mislocalization and abnormal and compartmentalized accumulation of several proteins involved in NCT function, some of which interact with ORF1p directly (KPNB1 and NUP153) or do not interact (i.e. RANgap1). KPNB1 sequestration by binding to ORF1p might alter nuclear import but could also inhibit its important disaggregase function [84]. Analogous, the abnormal localization of NUP153 in the nucleoplasm suggests an alteration of its physiological function, potentially mediated by the interaction with ORF1p as illustrated by the accumulation of nucleoplasmic PLA foci. Nucleoporins are long-lived proteins [85,86] and rely on cell division for their renewal. Post-mitotic neurons do not divide and nucleoporins therefore are not renewed [87,88]. Their continuous functioning in non-dividing cells throughout the life time of an individual is thus of crucial importance and any perturbations will have potentially irreversible consequences [87]. Indeed abnormal intranuclear and/or cytoplasmic accumulation of nucleoporins (such as NUP62, NUP88) have been described in the context of NDs (i.e, HD) [83]. Similarly, delocalization and abnormal cytoplasmic accumulation of RANgap1, a protein with GTPase activity involved in maintaining a RAN gradient required for NCT, have been described in ND-affected tissues [49].

NCT deficiencies have been consistently linked to the abnormal subcellular distribution of TDP-43, a nuclear protein involved in RNA metabolism [89,90], mutated in ALS/FTD [91–94] and mislocalized to the cytoplasm in numerous NDs [49–51] not linked to TDP-43 mutations. Indeed, in our model, NCT deficiencies as a consequence of mislocalized NCT proteins resulted in the cytoplasmic accumulation of TDP-43. TDP-43 exits the nucleus through passive [95] or active nuclear export [96] through nuclear pores. We also observed an increase in the nuclear pool which could be indicative of a perturbed export mechanism of this shuttling protein [97]. Together, our results suggest a possible scenario in which ORF1p might sequester and/or mislocalize NE components such as Lamin B1 or NUP153 (see below).

NE alteration and NCT defects are emerging pathogenic features in several NDs [77,98,99] including HD [81], ALS/FTD [82], PD [79], AD [98,99] and more generally in the context of tauopathies [100]. For example, aggregated Tau directly interacts with the nuclear pore complex [98] and oligomeric Tau with lamin proteins [101] resulting in loss of nuclear integrity including NCT failure [76], similar to what we describe here. Loss of nuclear integrity in the form of NE deformation and loss of NE function has been extensively described in the context of aging [102] including in the brain [103] with associated changes in chromatin organization and NCT dysfunction [99,103–105]. Progerin, a mutant form of lamin A, is the cause of the premature aging syndrome Hutchinson-Gilford progeria. Similar to mutant Tau, it accumulates at the NE and disrupts NE morphology, NCT and chromatin organization [56]. In cellular and mouse models of accelerated aging, these alterations can be successfully corrected by treatment with the small molecule Remodelin [56,57]. Remodelin acts by inhibiting the acetyltransferase NAT10 [56]. In our model of oxidative stress, pre-treatment of neurons with Remodelin 24 h prior to arsenite application restored, just as in progeria cells, NE abnormalities. In parallel, Remodelin decreased nuclear ORF1p while not affecting cytoplasmic ORF1p content. Remodelin might thus, through the restoration of the nuclear architecture, prevent ORF1p nuclear translocation and therefore further ORF1p-induced NE dysmorphology. Nuclear lamina-alterations do not only affect NCT but alter global chromatin organization [106] and potentially cell type specific gene expression [107]. Chromatin organization in cells is spatial and specific heterochromatin domains are directly linked to the nuclear lamina, called lamina-associated domains (LADs). One marker associated with LADs is H4K20me3, a repressive heterochromatin mark known to silence LINE-1 elements [59]. Indeed, oxidative stress induced a global loss of H4K20me3 which is rescued by Remodelin pre-treatment. Together, these data indicate that Remodelin can preserve and/or restore nuclear integrity of neurons including chromatin disorganization induced by oxidative stress possibly or at least partly through an inhibitory effect on ORF1p

nuclear translocation. The destructuration of nuclear lamina-anchored heterochromatin as indicated by the delocalization of H4K20me3 from the nuclear periphery could lead to the expression of genes normally repressed in post-mitotic neurons leading to neuronal fate loss, an emerging feature of aging and NDs [108]. Indeed, mutated Tau can lead to chromatin relaxation, re-expression of certain fetal genes in the brain in a fly model [18] and activation of TEs [14,18]. Further, the loss of H4K20me3 at the nuclear periphery could either be the source of LINE-1 activation (as H4K20me3 is a repressive mark known to decorate repeat DNA [109,110]) or the consequence of nuclear ORF1p translocation leading to a decrease in H4K20me3 through a yet to be identified mechanism. This would indeed lead to the amplification of the initial stress-induced increase in LINE-1 via a positive feedback loop. Another possibility is an adaptive response aimed at protecting the genome from damage as a short-term response to deformation [111–113].

Recent studies have shown that aggregated proteins such as Tau [71,114], mutant Huntingtin [81] and C9ORF72 poly(GA) [49] can target the NE and alter its integrity and function. Our data suggests that ORF1p might have a pathogenic action similar to ND-linked proteins by perturbing nuclear integrity. In addition, stress-granule independent cytoplasmic TDP-43 droplets can drive nuclear import defects and cell death [115]. Whether nuclear import defects are driven by a direct ORF1p dependent mechanism or via ORF1p-dependent TDP-43 cytoplasmic accumulation remains to be determined.

Condensation is a feature of ORF1p which is intrinsic to its role in LINE-1 mobilization [116]. We observed large ORF1p foci at the level of NE invaginations and an increase in the size of cytoplasmic and nuclear ORF1p foci (dots) indicative of ORF1p condensation. Whether ORF1p itself might be aggregation-prone or participate in the organization of LLPS (Liquid liquid phase separation)-related cytoplasmic or nuclear membraneless organelles requires further investigation.

In conclusion, we provide evidence that the LINE-1 encoded protein ORF1p, independent on the LINE-1 RNP or ORF2p, translocates to the nucleus upon cellular stress in an importin-beta and NUP153 involving process. Upon translocation, ORF1p binds to Lamin B1 and sequesters and/or mislocalizes this protein, which is essential to NE integrity, leading to further deformation of the NE. In parallel, while entering the nucleus through nuclear pores, ORF1p binds to NUP153, leading to its mislocalization to the nucleoplasm and thereby contributing to NCT deficiencies including the cytoplasmic accumulation of TDP-43. NE deformation is associated with chromatin disorganization as illustrated by HP1 loss at the inner NE and global H4K20me3 depletion in the nucleus. Nuclear deformation and chromatin disorganization upon cell stress were rescued by the small molecule Remodelin which might indirectly act as an inhibitor of ORF1p nuclear translocation. This suggests that that LINE-1 encoded protein ORF1p, for which no pathogenic function had yet been assigned, might play a pathogenic role by targeting the NE. As LINE-1 activation is a recurring observation in several neurological diseases [117–123], in the aging process [6] and more generally upon oxidative stress [5] and if this activation includes full-length LINE-1 elements with coding potential, the result could be an increase in ORF1p, in addition to ORF2p and LINE-1 RNA. Passing a certain threshold and in conjunction with a fragilization of the NE either through aging, ND-linked mutated proteins known to affect the NE or oxidative stress, this then might trigger the nuclear translocation of ORF1p contributing to NE deformation and NCT dysfunction. One consequence we identified is the cytoplasmic accumulation of TDP-43 which could favor its aggregation [124], one of the hallmarks of several NDs [49–51].

Activation of LINE-1 elements in neurons, through ORF2p-induced genomic instability [5], ORF2p-induced inflammation [6,8,44] or LINE-1 RNA mediated heterochromatin erosion [125] and, as we show here, through the ORF1-dependent fragilization of nuclear integrity could contribute in multiple ways to pathological features common to several NDs. This reinforces

the idea that LINE-1 elements might represent a novel therapeutic target for neuroprotection.

Acknowledgements

RZ acknowledges the Fondation Recherche Alzheimer (FRA) for a Ph.D. fellowship and is enrolled with the Ecole Doctorale ED3C at Sorbonne University. This work was supported by grants to JF from the Fondation de France (00086320), the Fondation du Collège de France, the Fondation NRJ/Institut de France and the National French Agency for Research (ANR-20-CE16-0022 NEURAGE). We gratefully acknowledge Julien Dumont and the Collège de France Orion imaging facility (IMACHEM-IBiSA), member of the French National Research Infrastructure France-BioImaging (ANR-10-INBS-04), which received support from the program «Investissements d'Avenir» ANR-10-LABX-54 MEMOLIFE. We also thank the Fondation Bettencourt Schueller for their support.

Author contributions

RZ performed most of the experiments. OMB contributed experimentally, PM and HM wrote the scripts for the automated image analysis workflow, RLJ and JF supervised the study and wrote the paper with RZ. JF received the funding.

Figure Legends

Figure 1. LINE-1 are upregulated in differentiated LUHMES cells following stress.

(A) Experimental paradigm of the differentiation scheme of LUHMES neuronal precursor cells into mature, post-mitotic dopaminergic neurons. At day 5 of differentiation, neurons were subjected to an oxidative stress using Arsenite ($NaAsO_2$). (B) After 5 days of differentiation, LUHMES cells express the neuronal marker Tuj1 and the dopaminergic marker TH as revealed by immunofluorescence. These neurons express LINE-1 at steady-state as shown by immunostaining for ORF1p protein. (C) Differentiated LUHMES neurons subjected to Arsenite treatment, show increased levels of ORF1p protein by Western blot analysis. n = 3 wells per condition from 4 independent experiments, mean ± SEM, Two-tailed t test. (D) Immunostaining for LINE-1 ORF1p of differentiated LUHMES cells treated with Arsenite and quantification of global ORF1p intensity, n > 100 neurons were quantified per condition, a representative experiment (3 wells per condition) of 3 independent experiments, mean ± SEM, Two-tailed t test. (E) Immunstaining of γH2AX following Arsenite treatment in the presence or the absence of Stavudine and quantification of γH2AX foci number in the nucleus. n > 100 neurons were quantified per condition, a representative experiment (3 wells per condition) of 2 independent experiments, mean ± SEM, One-way ANOVA with Tukey's multiple comparisons test (*p < 0.5, **p < 0.01, ***p < 0.001, ****p < 0.0001. (Also see supplementary Fig. 1). Scale bar, 5 μm.

Figure 2. ORF1p increases, changes its conformational pattern and translocates to the nucleus following oxidative stress.

(A) Immunostaining for LINE-1 ORF1p of differentiated LUHMES cells treated with Arsenite. (B) Quantification of ORF1p intensity both in the cytoplasm and the nucleus in the presence

and the absence of stress. n > 100 neurons were quantified per condition, a representative experiment (3 wells per condition) of 8 independent experiments, mean ± SEM, Two-tailed t test (C) Scheme of the script (for details see Materials and Methods) for ORF1p quantification in the cytoplasmic, nuclear (nucleoplasm = nucleus – inner NE) and inner and outer NE compartments. (D) Quantification of the number and volume of ORF1p positive dots shown in ROI (region of interest) (A) in the cytoplasm and the nucleus using the same script, n > 100 neurons were quantified per condition, a representative experiment (3 wells per condition) of 8 independent experiments, mean ± SEM, Two-tailed t test. Quantification of ORF1p signal at the nuclear envelope by an in-house script as schematized in (E) (for details see Materiel and Methods) shows increased ORF1p intensity at the inner NE and outer NE (F), n > 100 neurons were quantified per condition, a representative experiment (3 wells per condition) of 5 independent experiments, mean ± SEM, Two-tailed t test (*p < 0.5, **p < 0.01, ***p < 0.001, ****p < 0.0001. Scale bar, 5 μm.

Figure 3. ORF1p association with nuclear envelope components and nuclear transport proteins increases upon oxidative stress.

(A) Co-immunostaining of ORF1p and Lamin B1 reveals their colocalization (yellow). (B) Validation of ORF1p interaction with Lamin B1 by co-immunoprecipitation and Western-blotting. (C) Direct interaction of ORF1p with Lamin B1 was revealed by PLA and quantified in (D), n > 50 neurons were quantified per condition, (3 wells per condition) (E) Co-immunostaining of ORF1p and KPNB1 or NUP153. (F) Validation of a direct interaction between ORF1p and KPNB1 or NUP153 by PLA. The quantification in separate cellular compartments is shown in (G, H), n > 50 neurons were quantified per condition, (3 wells per condition), mean ± SEM, Two-tailed t test (*p < 0.5, **p < 0.01, ***p < 0.001, ****p < 0.0001. Scale bar, 5 μm.

Figure 4. Stress induced association of ORF1p to the nuclear envelope leads to nuclear envelope dysmorphology.

(A) Nuclear envelope dysmorphology in the Arsenite stress model revealed by co-immunostaining of ORF1p and LaminB1 quantified in (B). The pourcentage of deformed cells was quantified in > 10 images per condition, a representative experiment (3 wells per condition) of 3 independent experiments is shown, mean ± SEM, Two-tailed t test. (C) These deformations are paralleled by an increase of Lamin B1 at the inner NE and in the nucleoplasm. (D) Quantification of nuclear dysmorphology by analyzing nuclear circularity using a dedicated script (for details see Materiel and Methods) based on Lamin B1 as a mask, shows decreased circularity under stress conditions. n > 100 neurons were quantified per condition, a representative experiment (3 wells per condition) of 5 independent experiments, mean ± SEM, Two-tailed t test. (E) Correlation of ORF1p intensity per cell in the nucleus or at the inner NE with nuclear circularity. n > 100 neurons were quantified per condition, a representative experiment (3 wells per condition) of 3 independent experiments, mean ± SEM, Two-tailed t test. (F) Immunostaining of HP1 in stressed cells and the ratio of HP1 intensity in the nucleoplasm over the nuclear periphery (inner NE). n > 100 neurons were quantified per condition, a representative experiment (3 wells per condition) of 3 independent experiments, mean ± SEM, Two-tailed t test. (G) Immunostaining of H4K20me3 repressive histone mark in stressed and control cells and its quantification in the nucleus. n > 100 neurons were quantified per condition, a representative experiment (3 wells per condition) of 3 independent experiments, mean ± SEM, Two-tailed t test (*p < 0.5, **p < 0.01, ***p < 0.001, ****p < 0.0001). Scale bar, 5 μm.

Figure 5. Stress induced association of ORF1p with the nuclear envelope is accompanied by nucleo-cytoplasmic transport defect.

(A) Immunostaining of KPNB1 in oxidative stress conditions and quantification of the intensity levels, the number and the volume of dots in the cytoplasm. (B) Immunostaining of NPC protein RANgap1 in oxidative stress conditions and quantification of the intensity levels, the number and the volume of dots in the cytoplasm. (C) Immunostaining of TDP-43 in oxidative stress conditions and quantification of the intensity levels, the number and the volume of dots in the cytoplasm. (D) Immunostaining of NUP153 in oxidative stress conditions and quantification of the intensity levels in the nucleoplasm and the cytoplasm. $n > 100$ neurons were quantified per condition, a representative experiment (3 wells per condition) of 3 independent experiments, mean ± SEM, Two-tailed t test (*$p < 0.5$, **$p < 0.01$, ***$p < 0.001$, ****$p < 0.0001$. Scale bar, 5 μm.

Figure 6. LINE-1 over-expression following transfection leads to nuclear envelope deformation and nucleo-cytoplasmic transport defects in the absence of stress.

(A) Co-Immunostaining of HA and Lamin B1 in cells transfected with pcDNA3-ORF1-HA or with pGFP as a control. (B) Quantification of the nuclear circularity index, Lamin B1 intensity in the nucleoplasm and correlation of HA-ORF1p intensity per cell in the nucleus with nuclear circularity. $n > 90$ neurons were quantified per condition, a representative experiment (3 wells per condition) of 3 independent experiments, mean ± SEM, Two-tailed t test. (C) Immunostaining of HA and RANgap1 in cells transfected with pcDNA3-ORF1-HA or with pGFP as a control. (D) Quantification of cytoplasmic RANgap1 intensity in transfected cells with pHA-ORF1 or pGFP as a control. $n > 90$ neurons were quantified per condition (3 wells per condition), mean ± SEM, Two-tailed t test. (E) Immunostaining of HA and TDP-43 in cells transfected with pcDNA3-ORF1-HA or with pGFP as a control. (F) Quantification of

cytoplasmic and nuclear TDP-43 signal in cells transfected with pHA-ORF1 or pGFP as a control. n > 100 neurons were quantified per condition (3 wells per condition), mean ± SEM, Two-tailed t test (*p < 0.5, **p < 0.01, ***p < 0.001, ****p < 0.0001). Scale bar, 5 μm.

Figure 7. Restauration of nuclear alterations by the small molecule Remodelin

(A) Immunostaining of ORF1p, LaminB1 and H4k20me3 of neurons with or without Remodelin pre-treatment 24 h before addition of Arsenite or sham. (B) Quantification of nuclear circularity and Lamin B1 intensity in the nucleoplasm. (C) Quantification of ORF1p intensity in the nucleus, in the inner NE and in the cytoplasm. (D) Quantification of H4k20me3 intensity in the nucleus. n > 100 neurons were quantified per condition, a representative experiment (3 wells per condition) of 3 independent experiments, mean ± SEM, One-way ANOVA with Tukey's multiple comparisons test (*p < 0.5, **p < 0.01, ***p < 0.001, ****p < 0.0001). Scale bar, 5 μm.

References

1. International Human Genome Sequencing Consortium, Whitehead Institute for Biomedical Research, Center for Genome Research:, Lander, E.S., Linton, L.M., Birren, B., Nusbaum, C., Zody, M.C., Baldwin, J., Devon, K., Dewar, K., et al. (2001). Initial sequencing and analysis of the human genome. Nature *409*, 860–921. 10.1038/35057062.

2. Penzkofer, T., Jäger, M., Figlerowicz, M., Badge, R., Mundlos, S., Robinson, P.N., and Zemojtel, T. (2017). L1Base 2: more retrotransposition-active LINE-1s, more mammalian genomes. Nucleic Acids Res *45*, D68–D73. 10.1093/nar/gkw925.

3. Gasior, S.L., Wakeman, T.P., Xu, B., and Deininger, P.L. (2006). The Human LINE-1 Retrotransposon Creates DNA Double-strand Breaks. Journal of Molecular Biology *357*, 1383–1393. 10.1016/j.jmb.2006.01.089.

4. Belgnaoui, S.M., Gosden, R.G., Semmes, O.J., and Haoudi, A. (2006). Human LINE-1 retrotransposon induces DNA damage and apoptosis in cancer cells. Cancer Cell International *6*, 13. 10.1186/1475-2867-6-13.

5. Blaudin de Thé, F., Rekaik, H., Peze-Heidsieck, E., Massiani-Beaudoin, O., Joshi, R.L., Fuchs, J., and Prochiantz, A. (2018). Engrailed homeoprotein blocks degeneration in adult dopaminergic neurons through LINE-1 repression. EMBO J *37*. 10.15252/embj.201797374.

6. Simon, M., Van Meter, M., Ablaeva, J., Ke, Z., Gonzalez, R.S., Taguchi, T., De Cecco, M., Leonova, K.I., Kogan, V., Helfand, S.L., et al. (2019). LINE1 Derepression in Aged Wild-Type and SIRT6-Deficient Mice Drives Inflammation. Cell Metabolism *29*, 871-885.e5. 10.1016/j.cmet.2019.02.014.

7. Thomas, C.A., Tejwani, L., Trujillo, C.A., Negraes, P.D., Herai, R.H., Mesci, P., Macia, A., Crow, Y.J., and Muotri, A.R. (2017). Modeling of TREX1-Dependent Autoimmune Disease using Human Stem Cells Highlights L1 Accumulation as a Source of

Neuroinflammation. Cell Stem Cell *21*, 319-331.e8. 10.1016/j.stem.2017.07.009.

8. De Cecco, M., Ito, T., Petrashen, A.P., Elias, A.E., Skvir, N.J., Criscione, S.W., Caligiana, A., Brocculi, G., Adney, E.M., Boeke, J.D., et al. (2019). Author Correction: L1 drives IFN in senescent cells and promotes age-associated inflammation. Nature *572*, E5–E5. 10.1038/s41586-019-1350-9.

9. Douville, R., Liu, J., Rothstein, J., and Nath, A. (2011). Identification of active loci of a human endogenous retrovirus in neurons of patients with amyotrophic lateral sclerosis. Ann Neurol. *69*, 141–151. 10.1002/ana.22149.

10. Li, W., Jin, Y., Prazak, L., Hammell, M., and Dubnau, J. (2012). Transposable Elements in TDP-43-Mediated Neurodegenerative Disorders. PLoS ONE *7*, e44099. 10.1371/journal.pone.0044099.

11. Krug, L., Chatterjee, N., Borges-Monroy, R., Hearn, S., Liao, W.-W., Morrill, K., Prazak, L., Rozhkov, N., Theodorou, D., Hammell, M., et al. (2017). Retrotransposon activation contributes to neurodegeneration in a Drosophila TDP-43 model of ALS. PLoS Genet *13*, e1006635. 10.1371/journal.pgen.1006635.

12. Prudencio, M., Gonzales, P.K., Cook, C.N., Gendron, T.F., Daughrity, L.M., Song, Y., Ebbert, M.T.W., van Blitterswijk, M., Zhang, Y.-J., Jansen-West, K., et al. (2017). Repetitive element transcripts are elevated in the brain of C9orf72 ALS/FTLD patients. Human Molecular Genetics *26*, 3421–3431. 10.1093/hmg/ddx233.

13. Sun, W., Samimi, H., Gamez, M., Zare, H., and Frost, B. (2018). Pathogenic tau-induced piRNA depletion promotes neuronal death through transposable element dysregulation in neurodegenerative tauopathies. Nat Neurosci *21*, 1038–1048. 10.1038/s41593-018-0194-1.

14. Guo, C., Jeong, H.-H., Hsieh, Y.-C., Klein, H.-U., Bennett, D.A., De Jager, P.L., Liu, Z., and Shulman, J.M. (2018). Tau Activates Transposable Elements in Alzheimer's Disease. Cell Reports *23*, 2874–2880. 10.1016/j.celrep.2018.05.004.

15. Gan, L., Cookson, M.R., Petrucelli, L., and La Spada, A.R. (2018). Converging pathways in neurodegeneration, from genetics to mechanisms. Nat Neurosci *21*, 1300–1309. 10.1038/s41593-018-0237-7.

16. Fu, H., Hardy, J., and Duff, K.E. (2018). Selective vulnerability in neurodegenerative diseases. Nat Neurosci *21*, 1350–1358. 10.1038/s41593-018-0221-2.

17. Ravel-Godreuil, C., Massiani-Beaudoin, O., Mailly, P., Prochiantz, A., Joshi, R.L., and Fuchs, J. (2021). Perturbed DNA methylation by Gadd45b induces chromatin disorganization, DNA strand breaks and dopaminergic neuron death. iScience *24*, 102756. 10.1016/j.isci.2021.102756.

18. Frost, B., Hemberg, M., Lewis, J., and Feany, M.B. (2014). Tau promotes neurodegeneration through global chromatin relaxation. Nat Neurosci *17*, 357–366. 10.1038/nn.3639.

19. Rekaik, H., Blaudin de Thé, F.-X., Fuchs, J., Massiani-Beaudoin, O., Prochiantz, A., and Joshi, R.L. (2015). Engrailed Homeoprotein Protects Mesencephalic Dopaminergic Neurons from Oxidative Stress. Cell Reports *13*, 242–250. 10.1016/j.celrep.2015.08.076.

20. Peze-Heidsieck, E., Bonnifet, T., Znaidi, R., Ravel-Godreuil, C., Massiani-Beaudoin, O., Joshi, R.L., and Fuchs, J. (2022). Retrotransposons as a Source of DNA Damage in Neurodegeneration. Frontiers in Aging Neuroscience *13*.

21. Lotharius, J., Barg, S., Wiekop, P., Lundberg, C., Raymon, H.K., and Brundin, P. (2002). Effect of Mutant α-Synuclein on Dopamine Homeostasis in a New Human Mesencephalic Cell Line. Journal of Biological Chemistry *277*, 38884–38894. 10.1074/jbc.M205518200.

22. Lotharius, J., Falsig, J., Van Beek, J., Payne, S., Dringen, R., Brundin, P., and Leist, M. (2005). Progressive Degeneration of Human Mesencephalic Neuron-Derived Cells Triggered by Dopamine-Dependent Oxidative Stress Is Dependent on the Mixed-Lineage Kinase

Pathway. J. Neurosci. *25*, 6329–6342. 10.1523/JNEUROSCI.1746-05.2005.

23. Scholz, D., Pöltl, D., Genewsky, A., Weng, M., Waldmann, T., Schildknecht, S., and Leist, M. (2011). Rapid, complete and large-scale generation of post-mitotic neurons from the human LUHMES cell line: LUHMES as widely applicable neuronal model system. Journal of Neurochemistry *119*, 957–971. 10.1111/j.1471-4159.2011.07255.x.

24. Schindelin, J., Arganda-Carreras, I., Frise, E., Kaynig, V., Longair, M., Pietzsch, T., Preibisch, S., Rueden, C., Saalfeld, S., Schmid, B., et al. (2012). Fiji: an open-source platform for biological-image analysis. Nat Methods *9*, 676–682. 10.1038/nmeth.2019.

25. Linkert, M., Rueden, C.T., Allan, C., Burel, J.-M., Moore, W., Patterson, A., Loranger, B., Moore, J., Neves, C., MacDonald, D., et al. (2010). Metadata matters: access to image data in the real world. Journal of Cell Biology *189*, 777–782. 10.1083/jcb.201004104.

26. Ollion, J., Cochennec, J., Loll, F., Escudé, C., and Boudier, T. (2013). TANGO: a generic tool for high-throughput 3D image analysis for studying nuclear organization. Bioinformatics *29*, 1840–1841. 10.1093/bioinformatics/btt276.

27. Stringer, C., Wang, T., Michaelos, M., and Pachitariu, M. (2021). Cellpose: a generalist algorithm for cellular segmentation. Nature Methods *18*, 100–107.

28. Schmidt, U., Weigert, M., Broaddus, C., and Myers, G. (2018). Cell Detection with Star-Convex Polygons. In Medical Image Computing and Computer Assisted Intervention – MICCAI 2018 Lecture Notes in Computer Science., A. F. Frangi, J. A. Schnabel, C. Davatzikos, C. Alberola-López, and G. Fichtinger, eds. (Springer International Publishing), pp. 265–273. 10.1007/978-3-030-00934-2_30.

29. Haase, R., Royer, L.A., Steinbach, P., Schmidt, D., Dibrov, A., Schmidt, U., Weigert, M., Maghelli, N., Tomancak, P., Jug, F., et al. (2020). CLIJ: GPU-accelerated image processing for everyone. Nat Methods *17*, 5–6. 10.1038/s41592-019-0650-1.

30. Zhang, X., Yin, M., and Zhang, M. (2014). Cell-based assays for Parkinson's disease

using differentiated human LUHMES cells. Acta Pharmacol Sin *35*, 945–956. 10.1038/aps.2014.36.

31. Harris, G., Hogberg, H., Hartung, T., and Smirnova, L. (2017). 3D Differentiation of LUHMES Cell Line to Study Recovery and Delayed Neurotoxic Effects. Current Protocols in Toxicology *73*, 11.23.1-11.23.28. 10.1002/cptx.29.

32. Harischandra, D.S., Rokad, D., Ghaisas, S., Verma, S., Robertson, A., Jin, H., Anantharam, V., Kanthasamy, A., and Kanthasamy, A.G. (2020). Enhanced differentiation of human dopaminergic neuronal cell model for preclinical translational research in Parkinson's disease. Biochimica et Biophysica Acta (BBA) - Molecular Basis of Disease *1866*, 165533. 10.1016/j.bbadis.2019.165533.

33. Junqueira, V.B.C., Barros, S.B.M., Chan, S.S., Rodrigues, L., Giavarotti, L., Abud, R.L., and Deucher, G.P. (2004). Aging and oxidative stress. Molecular Aspects of Medicine *25*, 5–16. 10.1016/j.mam.2004.02.003.

34. Romano, A.D., Serviddio, G., de Matthaeis, A., Bellanti, F., and Vendemiale, G. (2010). Oxidative stress and aging. J Nephrol *23 Suppl 15*, S29-36.

35. Liguori, I., Russo, G., Curcio, F., Bulli, G., Aran, L., Della-Morte, D., Gargiulo, G., Testa, G., Cacciatore, F., Bonaduce, D., et al. (2018). Oxidative stress, aging, and diseases. CIA *Volume 13*, 757–772. 10.2147/CIA.S158513.

36. Hayes, J.D., Dinkova-Kostova, A.T., and Tew, K.D. (2020). Oxidative Stress in Cancer. Cancer Cell *38*, 167–197. 10.1016/j.ccell.2020.06.001.

37. Emerit, J., Edeas, M., and Bricaire, F. (2004). Neurodegenerative diseases and oxidative stress. Biomedicine & Pharmacotherapy *58*, 39–46. 10.1016/j.biopha.2003.11.004.

38. Chen, X., Guo, C., and Kong, J. (2012). Oxidative stress in neurodegenerative diseases. Neural Regen Res *7*, 376–385. 10.3969/j.issn.1673-5374.2012.05.009.

39. Kim, G.H., Kim, J.E., Rhie, S.J., and Yoon, S. (2015). The Role of Oxidative Stress in

Neurodegenerative Diseases. Exp Neurobiol *24*, 325–340. 10.5607/en.2015.24.4.325.

40. Fischer, R., and Maier, O. (2015). Interrelation of Oxidative Stress and Inflammation in Neurodegenerative Disease: Role of TNF. Oxidative Medicine and Cellular Longevity *2015*, e610813. 10.1155/2015/610813.

41. Giorgi, G., Marcantonio, P., and Del Re, B. (2011). LINE-1 retrotransposition in human neuroblastoma cells is affected by oxidative stress. Cell Tissue Res *346*, 383–391. 10.1007/s00441-011-1289-0.

42. Wongpaiboonwattana, W., Tosukhowong, P., Dissayabutra, T., Mutirangura, A., and Boonla, C. (2013). Oxidative Stress Induces Hypomethylation of LINE-1 and Hypermethylation of the RUNX3 Promoter in a Bladder Cancer Cell Line. Asian Pacific Journal of Cancer Prevention *14*, 3773–3778. 10.7314/APJCP.2013.14.6.3773.

43. Whongsiri, P., Pimratana, C., Wijitsettakul, U., Sanpavat, A., Jindatip, D., Hoffmann, M.J., Goering, W., Schulz, W.A., and Boonla, C. (2019). Oxidative stress and LINE-1 reactivation in bladder cancer are epigenetically linked through active chromatin formation. Free Radical Biology and Medicine *134*, 419–428. 10.1016/j.freeradbiomed.2019.01.031.

44. Thomas, C.A., Tejwani, L., Trujillo, C.A., Negraes, P.D., Herai, R.H., Mesci, P., Macia, A., Crow, Y.J., and Muotri, A.R. (2017). Modeling of TREX1-Dependent Autoimmune Disease using Human Stem Cells Highlights L1 Accumulation as a Source of Neuroinflammation. Cell Stem Cell *21*, 319-331.e8. 10.1016/j.stem.2017.07.009.

45. Mita, P., Wudzinska, A., Sun, X., Andrade, J., Nayak, S., Kahler, D.J., Badri, S., LaCava, J., Ueberheide, B., Yun, C.Y., et al. (2018). LINE-1 protein localization and functional dynamics during the cell cycle. eLife *7*, e30058. 10.7554/eLife.30058.

46. Freeman, B.T., Sokolowski, M., Roy-Engel, A.M., Smither, M.E., and Belancio, V.P. (2019). Identification of charged amino acids required for nuclear localization of human L1 ORF1 protein. Mobile DNA *10*, 20. 10.1186/s13100-019-0159-2.

47. Kapinos, L.E., Huang, B., Rencurel, C., and Lim, R.Y.H. (2017). Karyopherins regulate nuclear pore complex barrier and transport function. Journal of Cell Biology *216*, 3609–3624. 10.1083/jcb.201702092.

48. Idica, A., Sevrioukov, E.A., Zisoulis, D.G., Hamdorf, M., Daugaard, I., Kadandale, P., and Pedersen, I.M. (2017). MicroRNA miR-128 represses LINE-1 (L1) retrotransposition by down-regulating the nuclear import factor TNPO1. Journal of Biological Chemistry *292*, 20494–20508. 10.1074/jbc.M117.807677.

49. Zhang, K., Donnelly, C.J., Haeusler, A.R., Grima, J.C., Machamer, J.B., Steinwald, P., Daley, E.L., Miller, S.J., Cunningham, K.M., Vidensky, S., et al. (2015). The C9orf72 repeat expansion disrupts nucleocytoplasmic transport. Nature *525*, 56–61. 10.1038/nature14973.

50. Neumann, M., Sampathu, D.M., Kwong, L.K., Truax, A.C., Micsenyi, M.C., Chou, T.T., Bruce, J., Schuck, T., Grossman, M., Clark, C.M., et al. (2006). Ubiquitinated TDP-43 in Frontotemporal Lobar Degeneration and Amyotrophic Lateral Sclerosis. Science *314*, 130–133. 10.1126/science.1134108.

51. Aizawa, H., Yamashita, T., Kato, H., Kimura, T., and Kwak, S. (2019). Impaired Nucleoporins Are Present in Sporadic Amyotrophic Lateral Sclerosis Motor Neurons that Exhibit Mislocalization of the 43-kDa TAR DNA-Binding Protein. J Clin Neurol *15*, 62. 10.3988/jcn.2019.15.1.62.

52. Scaffidi, P., and Misteli, T. (2006). Lamin A-Dependent Nuclear Defects in Human Aging. Science *312*, 1059–1063. 10.1126/science.1127168.

53. Worman, H.J. (2012). Nuclear lamins and laminopathies. The Journal of Pathology *226*, 316–325. 10.1002/path.2999.

54. Stiekema, M., van Zandvoort, M.A.M.J., Ramaekers, F.C.S., and Broers, J.L.V. (2020). Structural and Mechanical Aberrations of the Nuclear Lamina in Disease. Cells *9*, 1884. 10.3390/cells9081884.

55. De Sandre-Giovannoli, A., Bernard, R., Cau, P., Navarro, C., Amiel, J., Boccaccio, I., Lyonnet, S., Stewart, C.L., Munnich, A., Le Merrer, M., et al. (2003). Lamin A Truncation in Hutchinson-Gilford Progeria. Science *300*, 2055–2055. 10.1126/science.1084125.

56. Larrieu, D., Viré, E., Robson, S., Breusegem, S.Y., Kouzarides, T., and Jackson, S.P. (2018). Inhibition of the acetyltransferase NAT10 normalizes progeric and aging cells by rebalancing the Transportin-1 nuclear import pathway. Science Signaling *11*, eaar5401. 10.1126/scisignal.aar5401.

57. Larrieu, D., Britton, S., Demir, M., Rodriguez, R., and Jackson, S.P. (2014). Chemical Inhibition of NAT10 Corrects Defects of Laminopathic Cells. Science *344*, 527–532. 10.1126/science.1252651.

58. Rangasamy, D. (2013). Distinctive patterns of epigenetic marks are associated with promoter regions of mouse LINE-1 and LTR retrotransposons. Mobile DNA *4*, 27. 10.1186/1759-8753-4-27.

59. Ren, W., Fan, H., Grimm, S.A., Kim, J.J., Li, L., Guo, Y., Petell, C.J., Tan, X.-F., Zhang, Z.-M., Coan, J.P., et al. (2021). DNMT1 reads heterochromatic H4K20me3 to reinforce LINE-1 DNA methylation. Nat Commun *12*, 2490. 10.1038/s41467-021-22665-4.

60. Casale, A.M., Liguori, F., Ansaloni, F., Cappucci, U., Finaurini, S., Spirito, G., Persichetti, F., Sanges, R., Gustincich, S., and Piacentini, L. (2021). Transposable element activation promotes neurodegeneration in a Drosophila model of Huntington's disease. iScience *25*, 103702. 10.1016/j.isci.2021.103702.

61. Tam, O.H., Rozhkov, N.V., Shaw, R., Kim, D., Hubbard, I., Fennessey, S., Propp, N., Fagegaltier, D., Harris, B.T., Ostrow, L.W., et al. (2019). Postmortem Cortex Samples Identify Distinct Molecular Subtypes of ALS: Retrotransposon Activation, Oxidative Stress, and Activated Glia. Cell Reports *29*, 1164-1177.e5. 10.1016/j.celrep.2019.09.066.

62. Ravel-Godreuil, C., Znaidi, R., Bonnifet, T., Joshi, R.L., and Fuchs, J. (2021).

Transposable elements as new players in neurodegenerative diseases. FEBS Letters *595*, 2733–2755. 10.1002/1873-3468.14205.

63. Dai, L., LaCava, J., Taylor, M.S., and Boeke, J.D. (2014). Expression and detection of LINE-1 ORF-encoded proteins. Mobile Genetic Elements. 10.4161/mge.29319.

64. Rangasamy, D., Lenka, N., Ohms, S., Dahlstrom, J.E., Blackburn, A.C., and Board, P.G. (2015). Activation of LINE-1 Retrotransposon Increases the Risk of Epithelial-Mesenchymal Transition and Metastasis in Epithelial Cancer. Current Molecular Medicine *15*, 588–597.

65. Macia, A., Widmann, T.J., Heras, S.R., Ayllon, V., Sanchez, L., Benkaddour-Boumzaouad, M., Muñoz-Lopez, M., Rubio, A., Amador-Cubero, S., Blanco-Jimenez, E., et al. (2017). Engineered LINE-1 retrotransposition in nondividing human neurons. Genome Res. *27*, 335–348. 10.1101/gr.206805.116.

66. Sur, D., Kustwar, R.K., Budania, S., Mahadevan, A., Hancks, D.C., Yadav, V., Shankar, S.K., and Mandal, P.K. (2017). Detection of the LINE-1 retrotransposon RNA-binding protein ORF1p in different anatomical regions of the human brain. Mobile DNA *8*, 17. 10.1186/s13100-017-0101-4.

67. Pereira, G.C., Sanchez, L., Schaughency, P.M., Rubio-Roldán, A., Choi, J.A., Planet, E., Batra, R., Turelli, P., Trono, D., Ostrow, L.W., et al. (2018). Properties of LINE-1 proteins and repeat element expression in the context of amyotrophic lateral sclerosis. Mobile DNA *9*, 35. 10.1186/s13100-018-0138-z.

68. Twyffels, L., Gueydan, C., and Kruys, V. (2014). Transportin-1 and Transportin-2: Protein nuclear import and beyond. FEBS Letters *588*, 1857–1868. 10.1016/j.febslet.2014.04.023.

69. Kimura, M., Okumura, N., Kose, S., Takao, T., and Imamoto, N. (2013). Identification of Cargo Proteins Specific for Importin-β with Importin-α Applying a Stable Isotope Labeling

by Amino Acids in Cell Culture (SILAC)-based in Vitro Transport System *. Journal of Biological Chemistry *288*, 24540–24549. 10.1074/jbc.M113.489286.

70. Manhas, S., Ma, L., and Measday, V. (2018). The yeast Ty1 retrotransposon requires components of the nuclear pore complex for transcription and genomic integration. Nucleic Acids Research *46*, 3552–3578. 10.1093/nar/gky109.

71. Candia, R.F., Cohen, L.S., Morozova, V., Corbo, C., and Alonso, A.D. (2022). Importin-Mediated Pathological Tau Nuclear Translocation Causes Disruption of the Nuclear Lamina, TDP-43 Mislocalization and Cell Death. Frontiers in Molecular Neuroscience *15*.

72. Ando, Y., Tomaru, Y., Morinaga, A., Burroughs, A.M., Kawaji, H., Kubosaki, A., Kimura, R., Tagata, M., Ino, Y., Hirano, H., et al. (2011). Nuclear Pore Complex Protein Mediated Nuclear Localization of Dicer Protein in Human Cells. PLoS ONE *6*, e23385. 10.1371/journal.pone.0023385.

73. Walther, T.C., Fornerod, M., Pickersgill, H., Goldberg, M., Allen, T.D., and Mattaj, I.W. (2001). The nucleoporin Nup153 is required for nuclear pore basket formation, nuclear pore complex anchoring and import of a subset of nuclear proteins. The EMBO Journal *20*, 5703–5714. 10.1093/emboj/20.20.5703.

74. Arora, R., Bodak, M., Penouty, L., Hackman, C., and Ciaudo, C. (2022). Sequestration of LINE -1 in cytosolic aggregates by MOV10 restricts retrotransposition. EMBO Reports *23*, e54458. 10.15252/embr.202154458.

75. Briggs, E.M., McKerrow, W., Mita, P., Boeke, J.D., Logan, S.K., and Fenyö, D. (2021). RIP-seq reveals LINE-1 ORF1p association with p-body enriched mRNAs. Mob DNA *12*, 5. 10.1186/s13100-021-00233-3.

76. Paonessa, F., Evans, L.D., Solanki, R., Larrieu, D., Wray, S., Hardy, J., Jackson, S.P., and Livesey, F.J. (2019). Microtubules Deform the Nuclear Membrane and Disrupt Nucleocytoplasmic Transport in Tau-Mediated Frontotemporal Dementia. Cell Reports *26*,

582-593.e5. 10.1016/j.celrep.2018.12.085.

77. Kim, H.J., and Taylor, J.P. (2017). Lost in Transportation: Nucleocytoplasmic Transport Defects in ALS and Other Neurodegenerative Diseases. Neuron *96*, 285–297. 10.1016/j.neuron.2017.07.029.

78. Kinoshita, Y., Ito, H., Hirano, A., Fujita, K., Wate, R., Nakamura, M., Kaneko, S., Nakano, S., and Kusaka, H. (2009). Nuclear Contour Irregularity and Abnormal Transporter Protein Distribution in Anterior Horn Cells in Amyotrophic Lateral Sclerosis. Journal of Neuropathology & Experimental Neurology *68*, 1184–1192. 10.1097/NEN.0b013e3181bc3bec.

79. Liu, S., Sawada, T., Lee, S., Yu, W., Silverio, G., Alapatt, P., Millan, I., Shen, A., Saxton, W., Kanao, T., et al. (2012). Parkinson's Disease–Associated Kinase PINK1 Regulates Miro Protein Level and Axonal Transport of Mitochondria. PLoS Genet *8*, e1002537. 10.1371/journal.pgen.1002537.

80. Sheffield, L.G., Miskiewicz, H.B., Tannenbaum, L.B., and Mirra, S.S. (2006). Nuclear Pore Complex Proteins in Alzheimer Disease. Journal of Neuropathology & Experimental Neurology *65*, 45–54. 10.1097/01.jnen.0000195939.40410.08.

81. Gasset-Rosa, F., Chillon-Marinas, C., Goginashvili, A., Atwal, R.S., Artates, J.W., Tabet, R., Wheeler, V.C., Bang, A.G., Cleveland, D.W., and Lagier-Tourenne, C. (2017). Polyglutamine-Expanded Huntingtin Exacerbates Age-Related Disruption of Nuclear Integrity and Nucleocytoplasmic Transport. Neuron *94*, 48-57.e4. 10.1016/j.neuron.2017.03.027.

82. Chou, C.-C., Zhang, Y., Umoh, M.E., Vaughan, S.W., Lorenzini, I., Liu, F., Sayegh, M., Donlin-Asp, P.G., Chen, Y.H., Duong, D.M., et al. (2018). TDP-43 pathology disrupts nuclear pore complexes and nucleocytoplasmic transport in ALS/FTD. Nat Neurosci *21*, 228–239. 10.1038/s41593-017-0047-3.

83. Grima, J.C., Daigle, J.G., Arbez, N., Cunningham, K.C., Zhang, K., Ochaba, J., Geater,

C., Morozko, E., Stocksdale, J., Glatzer, J.C., et al. (2017). Mutant Huntingtin Disrupts the Nuclear Pore Complex. Neuron *94*, 93-107.e6. 10.1016/j.neuron.2017.03.023.

84. Guo, L., Fare, C.M., and Shorter, J. (2019). Therapeutic Dissolution of Aberrant Phases by Nuclear-Import Receptors. Trends in Cell Biology *29*, 308–322. 10.1016/j.tcb.2018.12.004.

85. Savas, J.N., Toyama, B.H., Xu, T., Yates, J.R., and Hetzer, M.W. (2012). Extremely Long-Lived Nuclear Pore Proteins in the Rat Brain. Science *335*, 942–942. 10.1126/science.1217421.

86. Toyama, B.H., Savas, J.N., Park, S.K., Harris, M.S., Ingolia, N.T., Yates, J.R., and Hetzer, M.W. (2013). Identification of Long-Lived Proteins Reveals Exceptional Stability of Essential Cellular Structures. Cell *154*, 971–982. 10.1016/j.cell.2013.07.037.

87. D'Angelo, M.A., Raices, M., Panowski, S.H., and Hetzer, M.W. (2009). Age-Dependent Deterioration of Nuclear Pore Complexes Causes a Loss of Nuclear Integrity in Postmitotic Cells. Cell *136*, 284–295. 10.1016/j.cell.2008.11.037.

88. Hetzer, M.W. (2010). The Nuclear Envelope. Cold Spring Harbor Perspectives in Biology *2*, a000539–a000539. 10.1101/cshperspect.a000539.

89. Buratti, E., and Baralle, F.E. (2010). The multiple roles of TDP-43 in pre-mRNA processing and gene expression regulation. RNA Biology *7*, 420–429. 10.4161/rna.7.4.12205.

90. Colombrita, C., Onesto, E., Megiorni, F., Pizzuti, A., Baralle, F.E., Buratti, E., Silani, V., and Ratti, A. (2012). TDP-43 and FUS RNA-binding Proteins Bind Distinct Sets of Cytoplasmic Messenger RNAs and Differently Regulate Their Post-transcriptional Fate in Motoneuron-like Cells. Journal of Biological Chemistry *287*, 15635–15647. 10.1074/jbc.M111.333450.

91. Barmada, S.J., Skibinski, G., Korb, E., Rao, E.J., Wu, J.Y., and Finkbeiner, S. (2010). Cytoplasmic Mislocalization of TDP-43 Is Toxic to Neurons and Enhanced by a Mutation Associated with Familial Amyotrophic Lateral Sclerosis. J. Neurosci. *30*, 639–649.

10.1523/JNEUROSCI.4988-09.2010.

92. Benajiba, L., Le Ber, I., Camuzat, A., Lacoste, M., Thomas-Anterion, C., Couratier, P., Legallic, S., Salachas, F., Hannequin, D., Decousus, M., et al. (2009). TARDBP mutations in motoneuron disease with frontotemporal lobar degeneration. Annals of Neurology *65*, 470–473. 10.1002/ana.21612.

93. Kabashi, E., Valdmanis, P.N., Dion, P., Spiegelman, D., McConkey, B.J., Velde, C.V., Bouchard, J.-P., Lacomblez, L., Pochigaeva, K., Salachas, F., et al. (2008). TARDBP mutations in individuals with sporadic and familial amyotrophic lateral sclerosis. Nat Genet *40*, 572–574. 10.1038/ng.132.

94. Sreedharan, J., Blair, I.P., Tripathi, V.B., Hu, X., Vance, C., Rogelj, B., Ackerley, S., Durnall, J.C., Williams, K.L., Buratti, E., et al. (2008). TDP-43 Mutations in Familial and Sporadic Amyotrophic Lateral Sclerosis. Science *319*, 1668–1672. 10.1126/science.1154584.

95. Duan, L., Zaepfel, B.L., Aksenova, V., Dasso, M., Rothstein, J.D., Kalab, P., and Hayes, L.R. (2022). Nuclear RNA binding regulates TDP-43 nuclear localization and passive nuclear export. Cell Reports *40*, 111106. 10.1016/j.celrep.2022.111106.

96. Winton, M.J., Igaz, L.M., Wong, M.M., Kwong, L.K., Trojanowski, J.Q., and Lee, V.M.-Y. (2008). Disturbance of Nuclear and Cytoplasmic TAR DNA-binding Protein (TDP-43) Induces Disease-like Redistribution, Sequestration, and Aggregate Formation *. Journal of Biological Chemistry *283*, 13302–13309. 10.1074/jbc.M800342200.

97. Ederle, H., and Dormann, D. (2017). TDP-43 and FUS *en route* from the nucleus to the cytoplasm. FEBS Lett *591*, 1489–1507. 10.1002/1873-3468.12646.

98. Eftekharzadeh, B., Daigle, J.G., Kapinos, L.E., Coyne, A., Schiantarelli, J., Carlomagno, Y., Cook, C., Miller, S.J., Dujardin, S., Amaral, A.S., et al. (2018). Tau Protein Disrupts Nucleocytoplasmic Transport in Alzheimer's Disease. Neuron *99*, 925-940.e7. 10.1016/j.neuron.2018.07.039.

99. Frost, B. (2016). Alzheimer's disease: An acquired neurodegenerative laminopathy. Nucleus *7*, 275–283. 10.1080/19491034.2016.1183859.

100. Prissette, M., Fury, W., Koss, M., Racioppi, C., Fedorova, D., Dragileva, E., Clarke, G., Pohl, T., Dugan, J., Ahrens, D., et al. (2022). Disruption of nuclear envelope integrity as a possible initiating event in tauopathies. Cell Reports *40*, 111249. 10.1016/j.celrep.2022.111249.

101. Jiang, L., and Wolozin, B. (2021). Oligomeric tau disrupts nuclear envelope via binding to lamin proteins and lamin B receptor. Alzheimer's & Dementia *17*, e054521. 10.1002/alz.054521.

102. Martins, F., Sousa, J., Pereira, C.D., da Cruz e Silva, O.A.B., and Rebelo, S. (2020). Nuclear envelope dysfunction and its contribution to the aging process. Aging Cell *19*, e13143. 10.1111/acel.13143.

103. Mertens, J., Paquola, A.C.M., Ku, M., Hatch, E., Böhnke, L., Ladjevardi, S., McGrath, S., Campbell, B., Lee, H., Herdy, J.R., et al. (2015). Directly Reprogrammed Human Neurons Retain Aging-Associated Transcriptomic Signatures and Reveal Age-Related Nucleocytoplasmic Defects. Cell Stem Cell *17*, 705–718. 10.1016/j.stem.2015.09.001.

104. Oberdoerffer, P., and Sinclair, D.A. (2007). The role of nuclear architecture in genomic instability and ageing. Nat Rev Mol Cell Biol *8*, 692–702. 10.1038/nrm2238.

105. Jovičić, A., Mertens, J., Boeynaems, S., Bogaert, E., Chai, N., Yamada, S.B., Paul, J.W., Sun, S., Herdy, J.R., Bieri, G., et al. (2015). Modifiers of C9orf72 dipeptide repeat toxicity connect nucleocytoplasmic transport defects to FTD/ALS. Nat Neurosci *18*, 1226–1229. 10.1038/nn.4085.

106. Chang, L., Li, M., Shao, S., Li, C., Ai, S., Xue, B., Hou, Y., Zhang, Y., Li, R., Fan, X., et al. (2022). Nuclear peripheral chromatin-lamin B1 interaction is required for global integrity of chromatin architecture and dynamics in human cells. Protein & Cell *13*, 258–280.

10.1007/s13238-020-00794-8.

107. Perovanovic, J., Dell'Orso, S., Gnochi, V.F., Jaiswal, J.K., Sartorelli, V., Vigouroux, C., Mamchaoui, K., Mouly, V., Bonne, G., and Hoffman, E.P. (2016). Laminopathies disrupt epigenomic developmental programs and cell fate. Sci. Transl. Med. *8*. 10.1126/scitranslmed.aad4991.

108. Traxler, L., Lucciola, R., Herdy, J.R., Jones, J.R., Mertens, J., and Gage, F.H. (2023). Neural cell state shifts and fate loss in ageing and age-related diseases. Nat Rev Neurol *19*, 434–443. 10.1038/s41582-023-00815-0.

109. Richards, E.J., and Elgin, S.C.R. (2002). Epigenetic Codes for Heterochromatin Formation and Silencing. Cell *108*, 489–500. 10.1016/S0092-8674(02)00644-X.

110. Black, J.C., Van Rechem, C., and Whetstine, J.R. (2012). Histone Lysine Methylation Dynamics: Establishment, Regulation, and Biological Impact. Molecular Cell *48*, 491–507. 10.1016/j.molcel.2012.11.006.

111. Denais, C.M., Gilbert, R.M., Isermann, P., McGregor, A.L., Te Lindert, M., Weigelin, B., Davidson, P.M., Friedl, P., Wolf, K., and Lammerding, J. (2016). Nuclear envelope rupture and repair during cancer cell migration. Science *352*, 353–358. 10.1126/science.aad7297.

112. Nava, M.M., Miroshnikova, Y.A., Biggs, L.C., Whitefield, D.B., Metge, F., Boucas, J., Vihinen, H., Jokitalo, E., Li, X., García Arcos, J.M., et al. (2020). Heterochromatin-Driven Nuclear Softening Protects the Genome against Mechanical Stress-Induced Damage. Cell *181*, 800-817.e22. 10.1016/j.cell.2020.03.052.

113. Raab, M., Gentili, M., De Belly, H., Thiam, H.-R., Vargas, P., Jimenez, A.J., Lautenschlaeger, F., Voituriez, R., Lennon-Duménil, A.-M., Manel, N., et al. (2016). ESCRT III repairs nuclear envelope ruptures during cell migration to limit DNA damage and cell death. Science *352*, 359–362. 10.1126/science.aad7611.

114. Hochmair, J., Exner, C., Franck, M., Dominguez-Baquero, A., Diez, L., Brognaro, H.,

Kraushar, M., Mielke, T., Radbruch, H., Kaniyappan, S., et al. (2022). Biomolecular Tau condensation is linked to Tau accumulation at the nuclear envelope. 2022.01.24.477544. 10.1101/2022.01.24.477544.

115. Gasset-Rosa, F., Lu, S., Yu, H., Chen, C., Melamed, Z., Guo, L., Shorter, J., Da Cruz, S., and Cleveland, D.W. (2019). Cytoplasmic TDP-43 De-mixing Independent of Stress Granules Drives Inhibition of Nuclear Import, Loss of Nuclear TDP-43, and Cell Death. Neuron *102*, 339-357.e7. 10.1016/j.neuron.2019.02.038.

116. Sil, S. (2022). Condensation of LINE-1 Is Required for Retrotransposition.

117. Shpyleva, S., Melnyk, S., Pavliv, O., Pogribny, I., and Jill James, S. (2018). Overexpression of LINE-1 Retrotransposons in Autism Brain. Mol Neurobiol *55*, 1740–1749. 10.1007/s12035-017-0421-x.

118. Bundo, M., Toyoshima, M., Okada, Y., Akamatsu, W., Ueda, J., Nemoto-Miyauchi, T., Sunaga, F., Toritsuka, M., Ikawa, D., Kakita, A., et al. (2014). Increased L1 Retrotransposition in the Neuronal Genome in Schizophrenia. Neuron *81*, 306–313. 10.1016/j.neuron.2013.10.053.

119. Doyle, G.A., Crist, R.C., Karatas, E.T., Hammond, M.J., Ewing, A.D., Ferraro, T.N., Hahn, C.-G., and Berrettini, W.H. (2017). Analysis of LINE-1 Elements in DNA from Postmortem Brains of Individuals with Schizophrenia. Neuropsychopharmacol. *42*, 2602–2611. 10.1038/npp.2017.115.

120. Liu, S., Du, T., Liu, Z., Shen, Y., Xiu, J., and Xu, Q. (2016). Inverse changes in L1 retrotransposons between blood and brain in major depressive disorder. Sci Rep *6*, 37530. 10.1038/srep37530.

121. Muotri, A.R., Marchetto, M.C.N., Coufal, N.G., Oefner, R., Yeo, G., Nakashima, K., and Gage, F.H. (2010). L1 retrotransposition in neurons is modulated by MeCP2. Nature *468*, 443–446. 10.1038/nature09544.

122. Zhao, B., Wu, Q., Ye, A.Y., Guo, J., Zheng, X., Yang, X., Yan, L., Liu, Q.-R., Hyde, T.M., Wei, L., et al. (2019). Somatic LINE-1 retrotransposition in cortical neurons and non-brain tissues of Rett patients and healthy individuals. PLOS Genetics *15*, e1008043. 10.1371/journal.pgen.1008043.

123. Coufal, N.G., Garcia-Perez, J.L., Peng, G.E., Marchetto, M.C.N., Muotri, A.R., Mu, Y., Carson, C.T., Macia, A., Moran, J.V., and Gage, F.H. (2011). Ataxia telangiectasia mutated (ATM) modulates long interspersed element-1 (L1) retrotransposition in human neural stem cells. Proceedings of the National Academy of Sciences *108*, 20382–20387. 10.1073/pnas.1100273108.

124. Van Eersel, J., Ke, Y.D., Gladbach, A., Bi, M., Götz, J., Kril, J.J., and Ittner, L.M. (2011). Cytoplasmic Accumulation and Aggregation of TDP-43 upon Proteasome Inhibition in Cultured Neurons. PLoS ONE *6*, e22850. 10.1371/journal.pone.0022850.

125. Della Valle, F., Thimma, M.P., Caiazzo, M., Pulcrano, S., Celii, M., Adroub, S.A., Liu, P., Alanis-Lobato, G., Broccoli, V., and Orlando, V. (2020). Transdifferentiation of Mouse Embryonic Fibroblasts into Dopaminergic Neurons Reactivates LINE-1 Repetitive Elements. Stem Cell Reports *14*, 60–74. 10.1016/j.stemcr.2019.12.002.

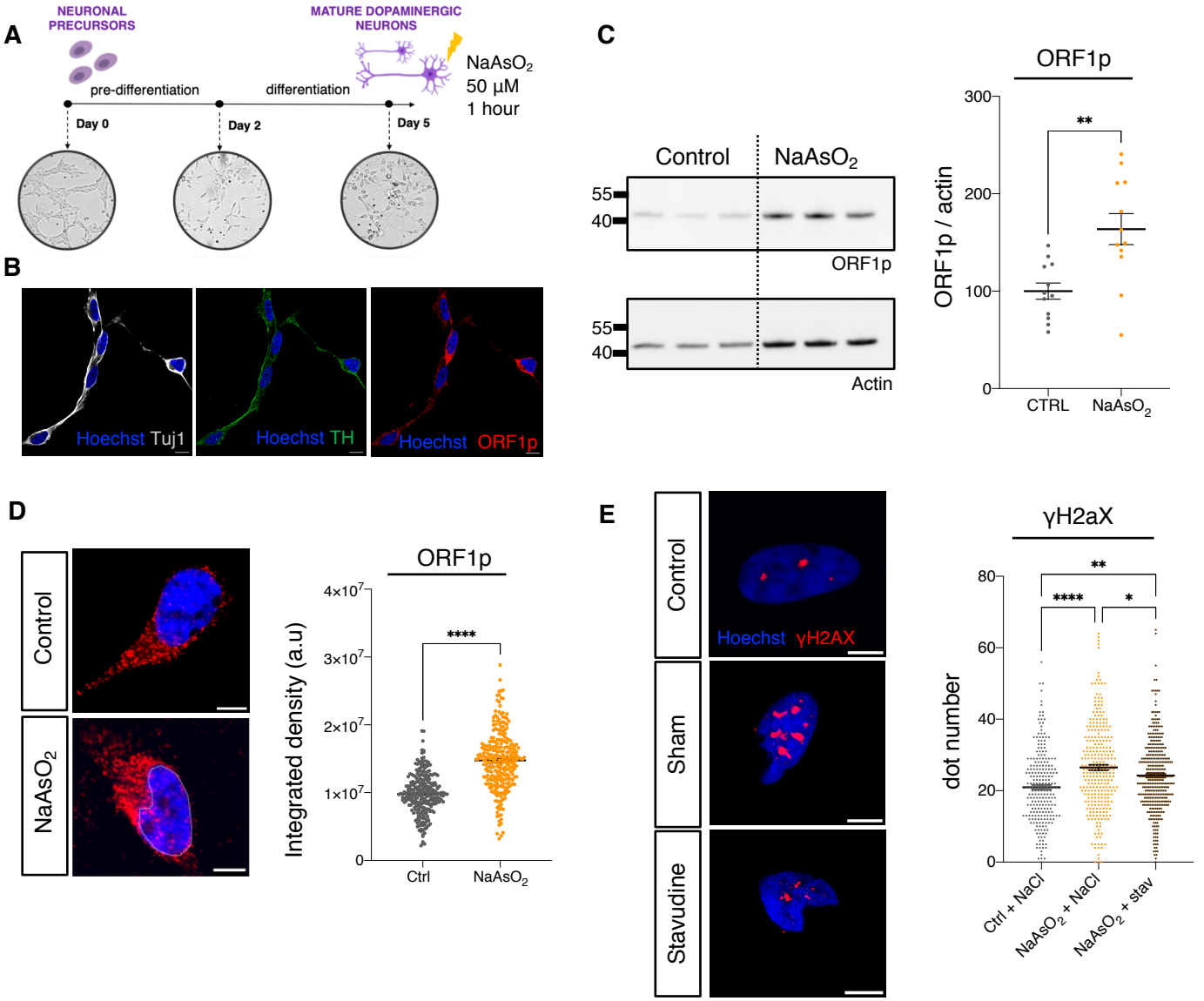
A
NEURONAL PRECURSORS
MATURE DOPAMINERGIC NEURONS
pre-differentiation
differentiation
Day 0
Day 2
Day 5
NaAsO2
50 µM
1 hour
B
Hoechst Tuj1
Hoechst TH
Hoechst ORF1p
C
Control
NaAsO2
55
40
ORF1p
55
40
Actin
ORF1p
ORF1p / actin
300
200
100
0
**
CTRL
NaAsO2
D
Control
NaAsO2
ORF1p
Integrated density (a.u)
4x10^7
3x10^7
2x10^7
1x10^7
0
****
Ctrl
NaAsO2
E
Control
Sham
Stavudine
Hoechst γH2AX
γH2aX
dot number
80
60
40
20
0
**
****
*
Ctrl + NaCl
NaAsO2 + NaCl
NaAsO2 + stav

Fig. 1

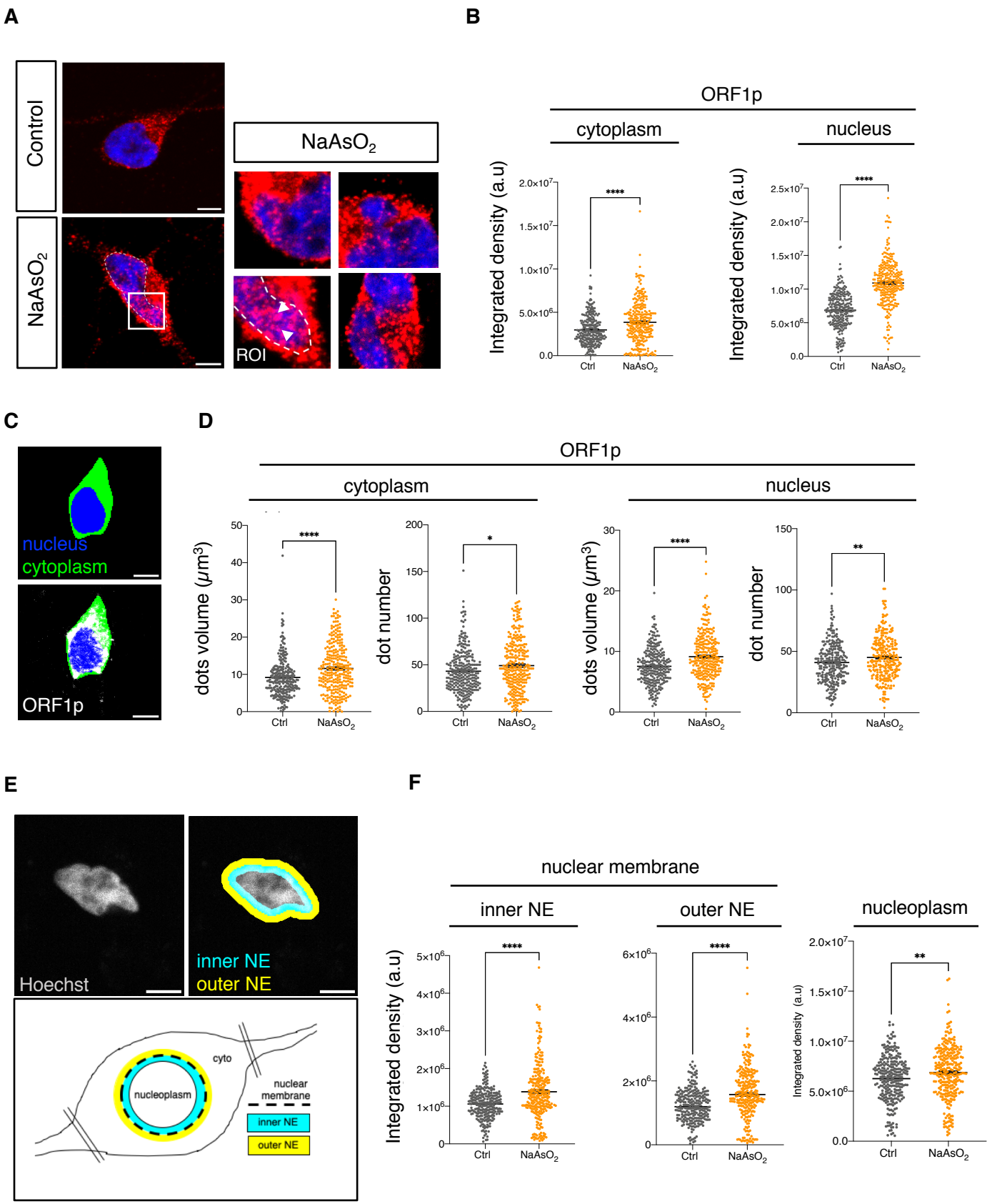
A
Control
NaAsO2
NaAsO2
ROI
B
ORF1p
cytoplasm
nucleus
Integrated density (a.u)
Ctrl
NaAsO2
C
nucleus
cytoplasm
ORF1p
D
ORF1p
cytoplasm
nucleus
dots volume (μm3)
dot number
E
Hoechst
inner NE
outer NE
cyto
nucleoplasm
nuclear membrane
inner NE
outer NE
F
nuclear membrane
inner NE
outer NE
nucleoplasm
Integrated density (a.u)

Fig. 2

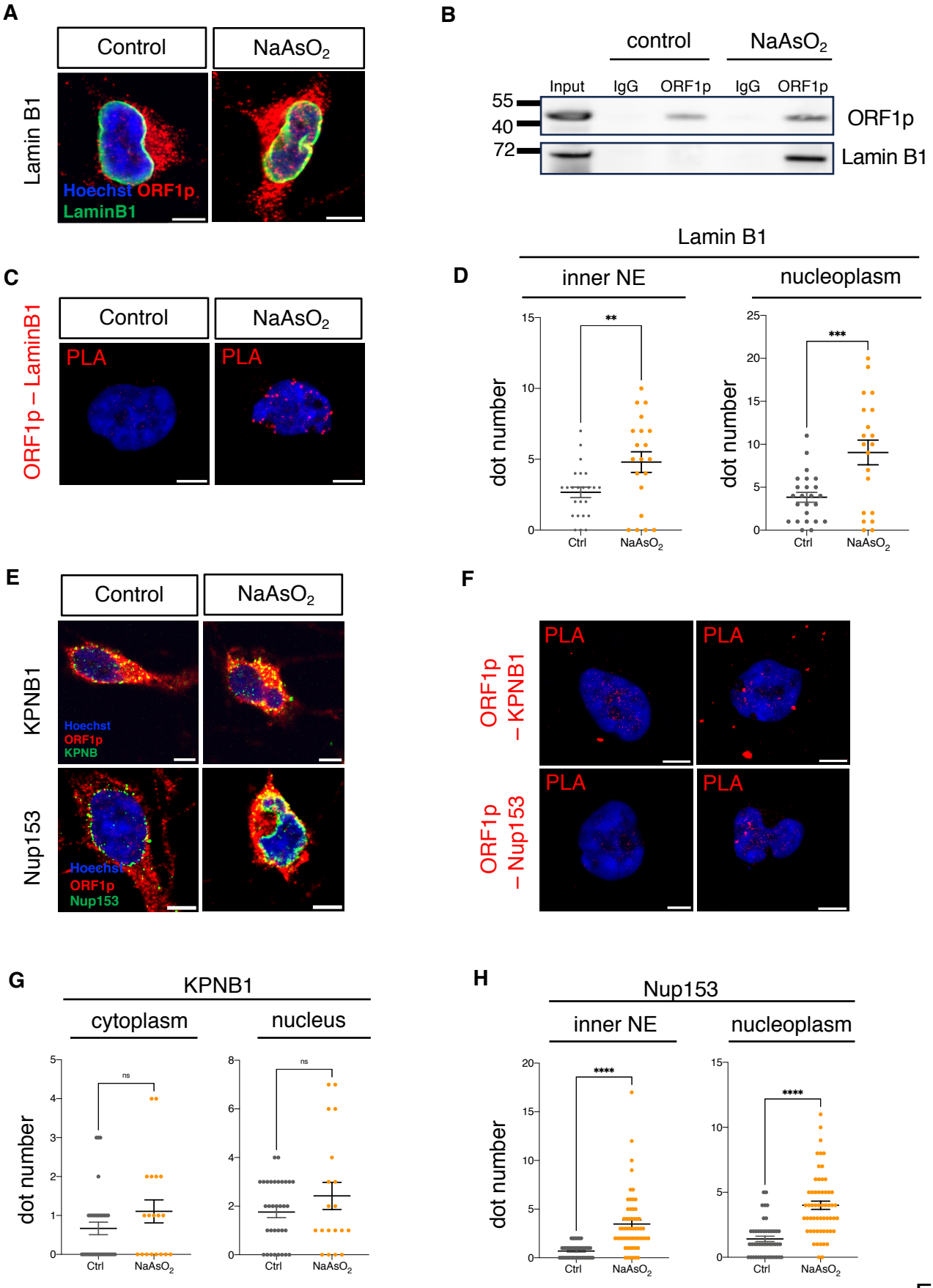
A
Control
NaAsO2
Lamin B1
Hoechst ORF1p
LaminB1
B
control
NaAsO2
Input
IgG
ORF1p
IgG
ORF1p
55
40
72
ORF1p
Lamin B1
C
Control
NaAsO2
ORF1p – LaminB1
PLA
PLA
D
Lamin B1
inner NE
nucleoplasm
dot number
**
***
Ctrl
NaAsO2
E
Control
NaAsO2
KPNB1
Hoechst
ORF1p
KPNB
Nup153
Hoechst
ORF1p
Nup153
F
ORF1p – KPNB1
ORF1p – Nup153
PLA
G
KPNB1
cytoplasm
nucleus
dot number
ns
H
Nup153
inner NE
nucleoplasm
dot number
****

Fig. 3

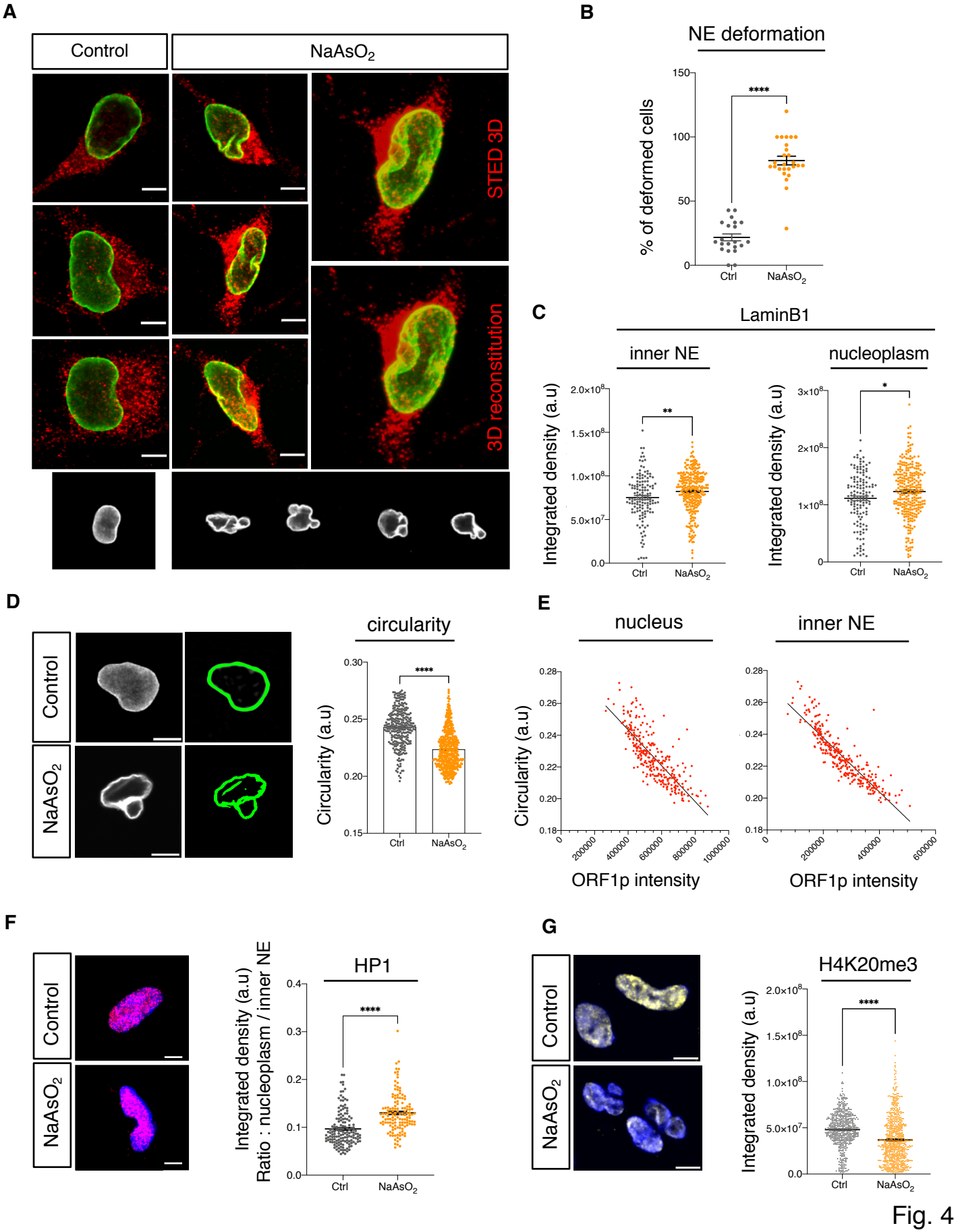
A
Control
NaAsO2
STED 3D
3D reconstitution
B
NE deformation
% of deformed cells
****
Ctrl
NaAsO2
C
LaminB1
inner NE
nucleoplasm
Integrated density (a.u)
**
*
D
Control
NaAsO2
circularity
Circularity (a.u)
****
E
nucleus
inner NE
Circularity (a.u)
ORF1p intensity
F
HP1
Integrated density (a.u)
Ratio : nucleoplasm / inner NE
G
H4K20me3
Integrated density (a.u)

Fig. 4

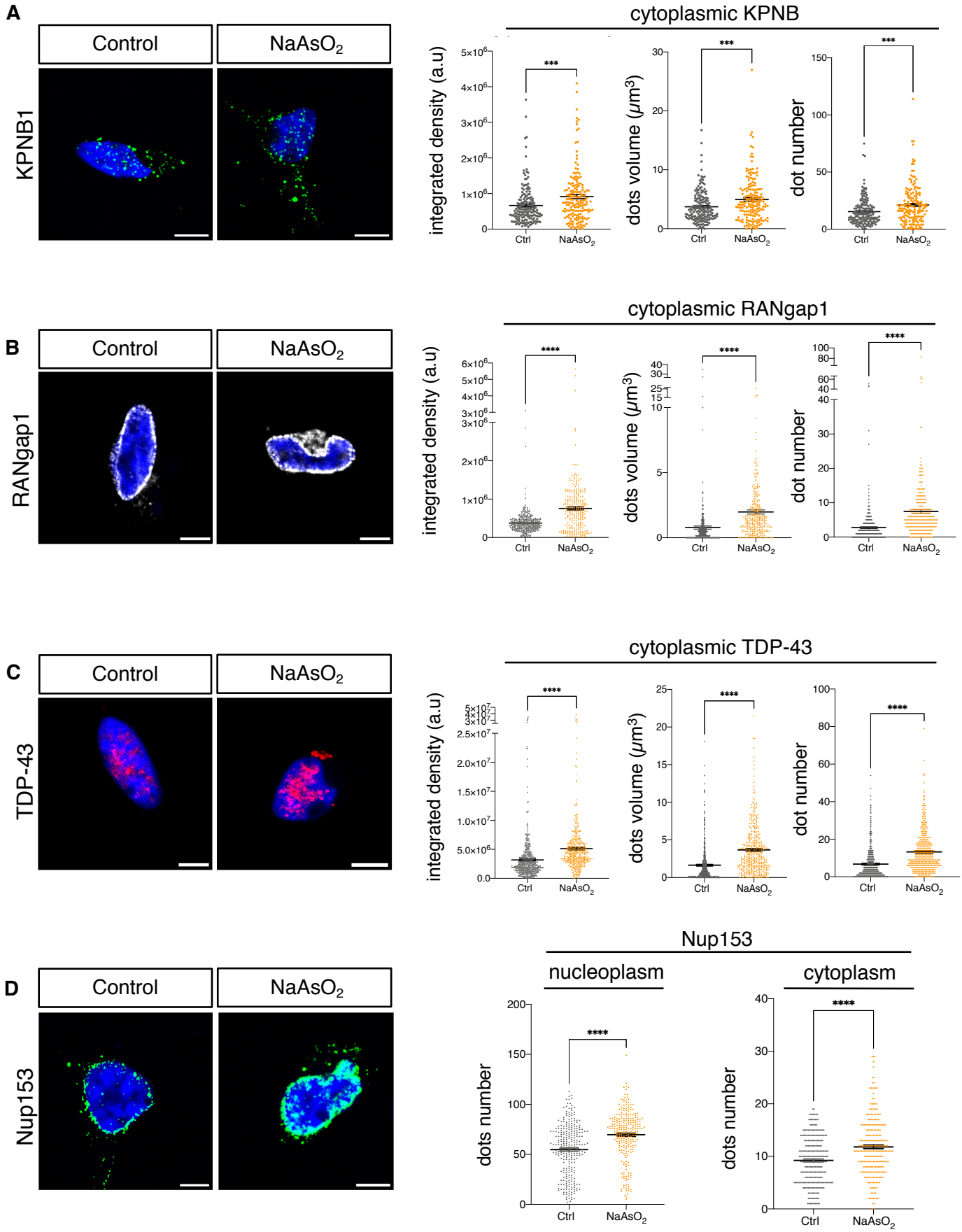
A
Control
NaAsO2
KPNB1
cytoplasmic KPNB
integrated density (a.u)
dots volume (μm3)
dot number
Ctrl
NaAsO2
B
RANgap1
cytoplasmic RANgap1
C
TDP-43
cytoplasmic TDP-43
D
Nup153
Nup153
nucleoplasm
cytoplasm
dots number

Fig. 5

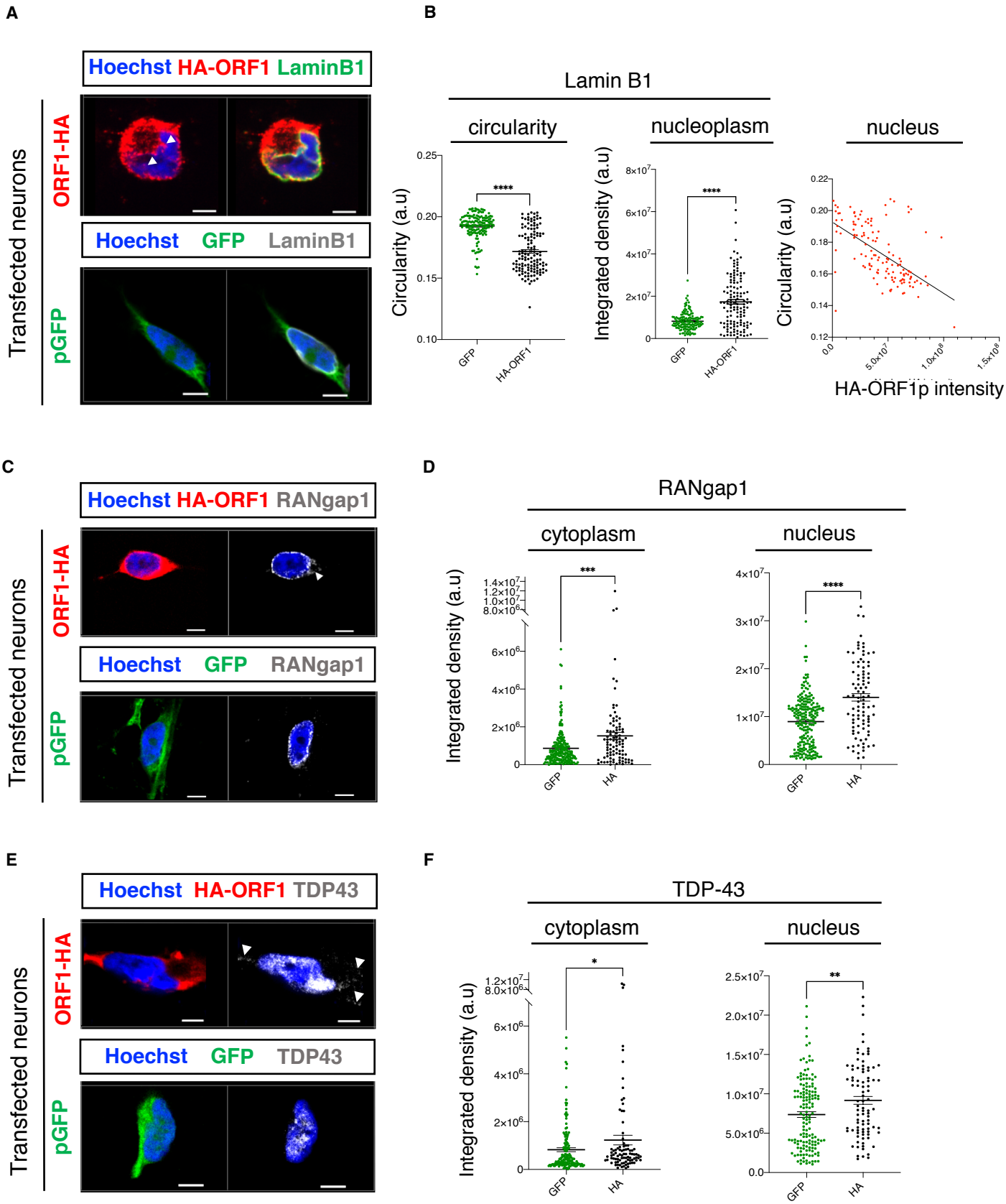
A
Hoechst HA-ORF1 LaminB1
Transfected neurons
ORF1-HA
Hoechst GFP LaminB1
pGFP
B
Lamin B1
circularity
nucleoplasm
nucleus
Circularity (a.u)
Integrated density (a.u)
Circularity (a.u)
GFP
HA-ORF1
HA-ORF1p intensity
C
Hoechst HA-ORF1 RANgap1
Transfected neurons
ORF1-HA
Hoechst GFP RANgap1
pGFP
D
RANgap1
cytoplasm
nucleus
Integrated density (a.u)
GFP
HA
E
Hoechst HA-ORF1 TDP43
Transfected neurons
ORF1-HA
Hoechst GFP TDP43
pGFP
F
TDP-43
cytoplasm
nucleus
Integrated density (a.u)
GFP
HA

Fig. 6

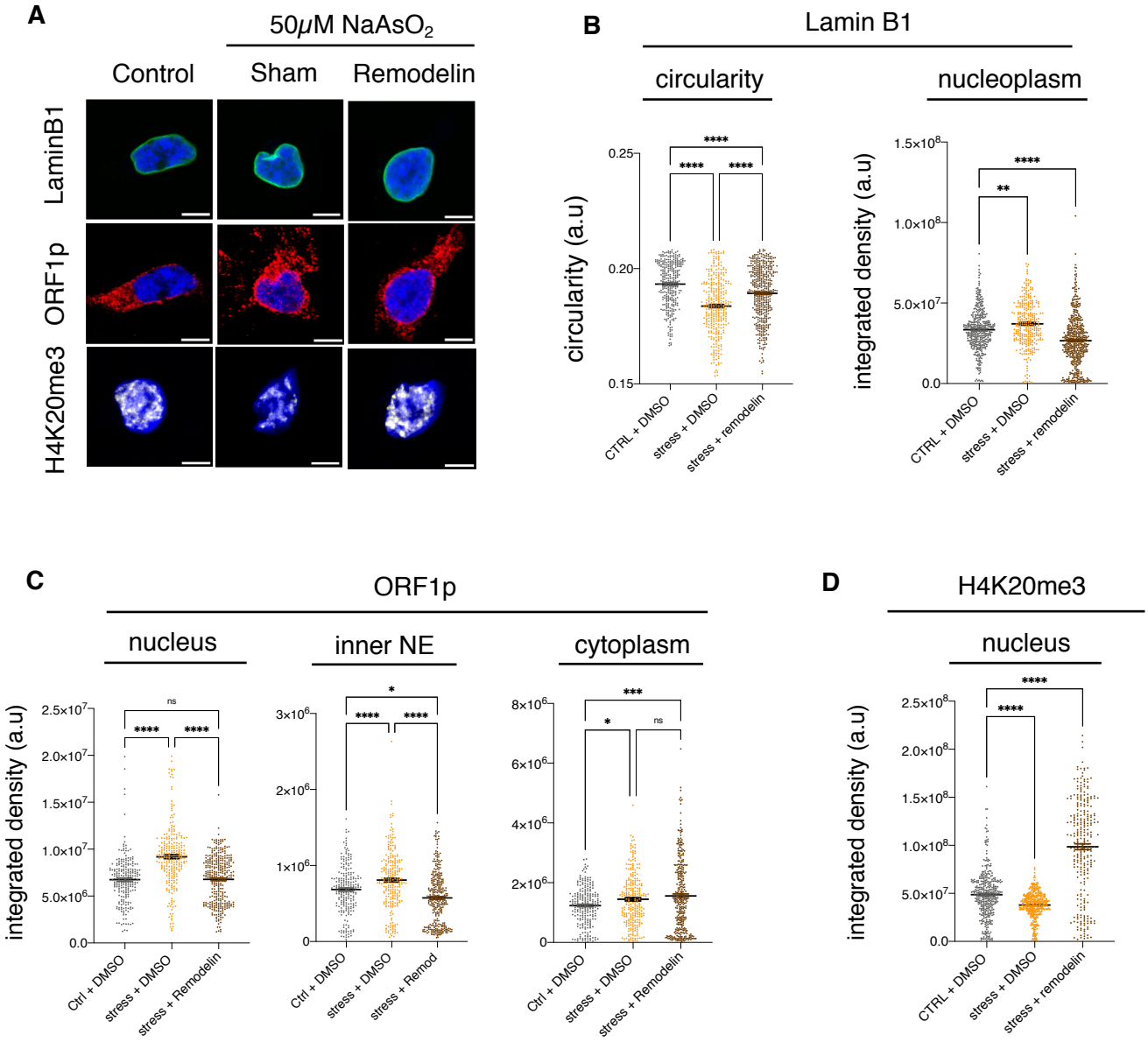
A
50μM NaAsO2
Control
Sham
Remodelin
LaminB1
ORF1p
H4K20me3
B
Lamin B1
circularity
nucleoplasm
circularity (a.u)
integrated density (a.u)
CTRL + DMSO
stress + DMSO
stress + remodelin
C
ORF1p
nucleus
inner NE
cytoplasm
integrated density (a.u)
Ctrl + DMSO
stress + DMSO
stress + Remodelin
stress + Remod
D
H4K20me3
nucleus
integrated density (a.u)
CTRL + DMSO
stress + DMSO
stress + remodelin

Fig. 7